KARADENİZ TECHNICAL UNIVERSITY
THE GRADUATE SCHOOL OF APPLIED SCIENCES

DEPARTMENT OF FOREST ENGINEERING

FOREST DYNAMICS IN MEDITERRANEAN FOREST USING LANSAT IMAGERY AND LIDAR

MASTER THESIS

Juan Jose MENA COSTA

APRIL 2016
TRABZON

KARADENİZ TECHNICAL UNIVERSITY

THE GRADUATE SCHOOL OF NATURAL AND APPLIED SCIENCES

DEPARMENT OF FOREST ENGİNEERİNG

FOREST DYNAMICS IN MEDITERRANEAN FOREST USING LANDSAT IMAGERY AND LIDAR

Juan Jose MENACOSTA

This thesis is accepted to give the degree of

"MASTER OF SCIENCE"

By

The Graduate School of Natural and Applied Sciences at Karadeniz Technical University

The Date of Submission : **22 / 03 /2016**

The Date of Examination : **19 / 04 /2016**

Supervisor : **Prof. Dr. Emin Zeki BAŞKENT**

Trabzon 2016

KARADENİZ TECHNICAL UNIVERSITY

THE GRADUATE SCHOOL OF NATURAL AND APPLIED SCIENCES

DEPARTMENT OF FOREST ENGINEERING

Juan Jose MENA COSTA

FOREST DYNAMICS IN MEDITERRANEAN FOREST USING LANDSAT IMAGERY AND LIDAR

Has been accepted as a thesis of

MASTER OF SCIENCE

after the Examination by the Jury Assigned by the Administrative Board of the Graduate School of Natural and Applied Sciences with the Decision Number 1645 dated 22 / 03 / 2016

Approved By

Chairman : Prof. Dr. Emin Zeki BAŞKENT .....

Member : Prof. Dr. Günay ÇAKIR .....

Member : Yrd. Doç. Dr. Uzay KARAHALİL .....

Prof. Dr. Sadettin KORKMAZ

Director of Graduate School

ACKNOWLEDGEMENTS

This thesis would not have been possible without the help of certain people. With immense gratitude, I acknowledge the support and help of my advisors Prof. Dr. José G. BORGES and Prof. Dr. Emin Zeki BAŞKENT

Also, I would like to express my special gratitude to my family for their help, for those many sleepless nights they stood by my side, and for their constant moral support. It is to my family, Bc. Ilona Endlicherová and my daughter Sofie Mena Endlicherová that this thesis is dedicated to.

Juan José Mena Costa

Trabzon

THESIS STATEMENT

I hereby declare that all information in this thesis titled as “Forest Dynamics in Mediterranean Forest Using Landsat Imagery and Lidar” has been completed under the responsibility of my supervisors Prof. Dr. José G. BORGES and Prof. Dr. Emin Zeki BAŞKENT and presented in accordance with academic rules and ethical conduct. I also declare that, as required by these rules and conduct, I have fully cited and referenced all material and results that are not original to this work 19.04.2016.

Juan José MENA COSTA

TABLE OF CONTENTS

Page Number

Yüksek Lisans

ÖZET

LANDSAT GÖRÜNTÜ ve LIDAR KULLANIMIYLA
AKDENİZ ORMANLARINDAKİ ORMAN DİNAMİĞİNİN ANALİZİ

Juan Jose MENA COSTA

Karadeniz Teknik Üniversitesi
Fen Bilimleri Enstitüsü
Orman Mühendisliği Anabilim Dalı
Danışman: Prof.. Dr. Emin Zeki BAŞKENT
2016, 71 Sayfa,

Akdeniz ormanları karmaşık ekosistemler olup süreçleri ve fonksiyonları yeterince bilinmemektedir. Uzaktan algılama teknikleri amenajman plan sonuçlarını izlemede kullanılmaktadır. 2009 yılından sonraki Landsat görüntüleri, vejetasyon indisleri ve LiDAR tabanlı değişkenler Random Forest modeline arazi bileşimi ve yapısını analiz etmek için entegre edilmiştir. Çalışma alanı, 2012 yılında yenilenmiş 1981 yılına ait eski bir amenajman planından alınmıştır. 1981, 1990, 2000, 2009, 2011 ve 2014 yılları için; orman-orman dışı ve çok sınıflı arazi kullanım haritalarının oluşturulmasında en iyi modeller üretilmiş ve kullanılmıştır. Tüm sınıflandırma modelleri oldukça iyi bir performans sunmuştur (Doğruluk >%85 , Kappa > 0.80). Çok sınıflı tasnif için en iyi performans %95.37 lik doğruluk ve 0.94 lük kappa değeriyle FUSION ile ulaşılmıştır. Binary sınıflandırması için; %98.5' i aşan doğruluk ve 0.96' yı aşan kappa indeksiyle LT, LVT ve FUSION ulaşmıştır. Biyomass üretimi odaklı orman amenajman planlarının uygulaması orman ekosistemlerinin yapı ve bileşimini değiştirdiği arazi indeksleri ile belirlenmiştir. Sonuçta, biyomas üretim ağırlıklı çam türlerine odaklanmış silvikültürel müdahalelerin arazinin doğal vejetasyonuna karşılık gelen meşe türlerine doğru araziyi değiştirdiği görülmüştür. Parça sayısının artması ve ortalama parça büyüklüğünün azalmasıyla çalışmaya konu alanın parçalı bir yapıya doğru gittiği sonucuna varılmıştır. Tep tacı yüksekliği ve kapalılık tahmininde RF kullanımı; CHM, CC ve HMAX için 0.563m, %6.99 ve 2.3 m lik RMSE ve 0.74 civarındaki doğruluk değerleri bulunduğu için orman dinamiğini açıklamada kuvvetli bir değişken olarak önerilmemektedir.

Anahtar Kelimeler: Orman Amenajmanı, Arazi dinamiği, LIDAR, Uzaktan algılama, Rassal orman

Master Thesis

SUMMARY

FOREST DYNAMICS IN MEDITERRANEAN FOREST
USING LANDSAT IMAGERY AND LIDAR

Juan Jose MENA COSTA

Karadeniz Technical University
The Graduate School of Natural and Applied Sciences
Forest Engineering Graduate Program
Supervisor: Prof. Dr.Emin Zeki BAŞKENT
2016, 71 Pages.

Twelve fungal strains including *Lecanicillium muscarium* (Petch.) Zare and Gams, *Isaria farinosa* (Holmsk.) Mediterranean forests are complex ecosystems and most aspects of their functioning are unknown. Remote sensing applications are used to monitoring the effect of forest management. The study area counted with an old management plan from 1981 which was reviewed in 2012. Six different databases built with Landsat bands, vegetation, tasseled cap transformations, LiDAR-based variables and topographic variables were used to assess the performance of Random Forest algorithm. Best of the models were used to produce forest-no forest and multiclass land cover maps for the years 1981, 1990, 2000, 2009, 2011 and 2014. Processes and patterns were analyzed using landscape metrics. Also RF regression models were assessed for prediction of canopy height model, canopy cover and maximum height for the same years. All classification models presented a very good performance (Accuracies > 85% with kappa > 0.80). For multiclass classification, the best performance was achieved by FUSION with 95.37% of accuracy and kappa 0.94. For binary classification LT, LVT and FUSION achieved more than 98.5% in accuracy and kappa index higher than 0.96. Results showed that the silvicultural activities focused on pine tree species for biomass production modify the landscape by recovering Holm oak species. The landscape in the study area became fragmented over the study period, because of the increase in the Number of Patches and the decrease in Mean Patch Area.Estimation of canopy height and canopy cover with the use of RF did not offer such a robust variable for explaining forest dynamics since the accuracies ranged about 0.74 with RMSE of 0.563m, 6.99% and 2.3m, for CHM, CC and HMAX, respectively.

Key Words: Forest Management, Landscape Dynamics, LiDAR, Remote sensing,Random forestl

LIST OF FIGURES

Page Number

LIST OF TABLES

Page Number

ACRONYMS

AGB	Above Ground Biomass
BLUE	Blue band
CC	Canopy cover
CHM	Mean canopy height
DEM	Digital Elevation Model
DN	Digital Numbers
DSM	Digital Surface Model
DTM	Digital Terrain Model
ETM+	Landsat Enhanced Thematic Mapper Plus
EVI	Enhanced Vegetation Index
ETRS	European Terrestrial Reference System
FUSION	LTV + LiDAR derived variables
GPS	Global Positioning System
HMAX	Maximum canopy height
IMAX	Maximum Intensity
LiDAR	Light Detection and Ranging
LLI	LV + LiDAR derived variables
LO	Reflective bands Landsat.
LT	Reflective bands Landsat + Topographic variables
LV	Reflective bands Landsat + Vegetation indices + Tasseled Cap components
LVT	LV + Topographic variables
LULC	Land Use/Land Cover
NDVI	Difference Vegetation Index
NIR	Near Infra Red
OLI	Landsat 8 Operational Land Imager
OOB	Out Of Bag
R	Red band
RF	Random Forest
SR	Simple Vegetation Ratio

SVMs	Support Vector Machines
TIRS	Landsat 8 Thermal Infrared Sensor
TM	Landsat Thematic Mapper
USGS	U.S. Geological Survey
UTM	Universal Transverse Mercator

1. INTRODUCTION

Mediterranean forests are complex ecosystems and, despite of its research, most aspects of their functioning are unknown. Experiments permit to obtain relatively fast results if compared with long-term monitoring, but are also costly, especially in forests, and their interpretation is rather complex because it is not possible to change just a variable at one time in the field (Terradas 2005). Nevertheless, qualitative models are often built to explore different attributes in order to gain knowledge to generate projections. To assess forest changes during the time is required to observe some variables over the time.

New technologies improved forest dynamics assessment during the last 3 decades. Since the launching of the first Landsat satellite (1972), the provided a relatively long historical record of remote sensing data in a moderate resolution. Imagery collected from the several sensors of the program has been proved useful for the forest cover characterization. One of the first works that dealt with forest-type mapping using remote sensing data was realized by Heller et al. (1974) and numerous studies have proceed with forest cover mapping and species differentiating (Coleman et al. 1990; Aardt & Wynne 2001).

Furthermore, the use of Landsat imagery is becoming popular since images are freely available in the USGS webpage. Different forest attributes have been related to the spectral signal received by the sensor as in Carreiras et al. (2006) where tree canopy cover was estimated in Mediterranean sclerofilous oak forests in Portugal. In Gómez et al. (2014) temporal spectral trajectories of Landsat images were used to estimate forest aboveground biomass in Mediterranean pine forests. In Vega-García & Chuvieco (2006) temporal vegetation spatial pattern was analyzed in Mediterranean mountainous landscape in order to predict fire occurrence.

In fact, the processing of the images may be done for classification purposes but also for estimation or regression. In Gong et al. (2013) a World-wide classification using Landsat presented the first Land Use/Land Cover (LULC) map with different levels of characters. But in Gómez et al. (2014) temporal spectral trajectories as unique source of data were used for modelling and mapping of historic AGB for Mediterranean pines in central Spain.

Light Detection and Ranging (LiDAR) technology provides a new perspective to the estimation of forest structure variables since offers direct information of the study area. It gives high resolution and georeferenced spatial data that have a particular utility in forest mapping. Cloud cover data can be processed to obtain directly a variety of canopy-structure variables such as canopy height, stand density, crown width and crown length (Leiterer et al. 2015). Also might be estimated parameters such as vegetation cover (Estornell et al. 2011), aboveground biomass and stem volume (Kankare et al. 2013). In (Næsset 2002) mean tree height, dominant height, mean diameter, stem number, basal area, and timber volume were estimated using LiDAR. But also with this kind of remote sensing data is possible to perform classification as in Garcia-Gutierrez et al. (2011). The usefulness of airborne LiDAR data for forest inventory parameters extraction is determined by the point density. Individual tree-level biomass mapping at regional scales is increasingly possible (Duncanson et al. 2015). Moreover, fusion satellite images with LiDAR have been proved to achieve more accurate results.

To further improve the performance of classification models different datasets are often combined with LiDAR data. In Shoemaker (2012) satellite data, LiDAR data and their combination were used to create a LULC with 6 classes. Fusion data using all LiDAR surface models improved class discrimination of spectrally similar forest, farmland, and managed clearings and produced the highest total accuracies at 1m, 5m, and 10m resolutions (87.2%, 86.3% and 85.4%, respectively). In Nourzad & Pradhan (2012) were achieved, nevertheless, very high accuracies 98.9% for binary and 94.6% for multi-class classification. Applying binary classification strategies such as one-against one or one against all, often increases accuracy, but only marginally (Chan et al. 2008). In Nourzad & Pradhan (2012) were achieved, nevertheless, very high accuracies 98.9% for binary and 94.6% for multi-class classification.

Computer models can significantly enhance our ability to address the issues of cause and effect relations on long temporal and broad spatial scales. In Pal (2005) was found that Random Forest classifier performs equally well to SVMs in terms of classification accuracy and training time and that the number of user-defined parameters required by random forest classifiers is less than the number required for SVMs and easier to define.

1.1. Objectives

The main purpose of this work is to determine the forest dynamic during the period of time comprised between 1984 to 2014 in both, composition and structure using fusion of Landsat satellite imagery, LiDAR and ancillary data. To achieve this goal was necessary to build some Random Forest models, assess their performance and choose the best, not only for classification purposes but also for the estimation of forest structural parameters such as canopy cover (CC), mean and maximum canopy height (CHM and HMAX). Finally, Landscape dynamics was assessed through landscape metrics derived from classification maps. The importance of the variables was also evaluated.

2. MATERIALS AND METHODS

2.1. Study Area

The study site of this work is the public forest num. V95 "Sierra Negrete". We choose this forest because its relatively recent management plan (2012) in Valencia province.

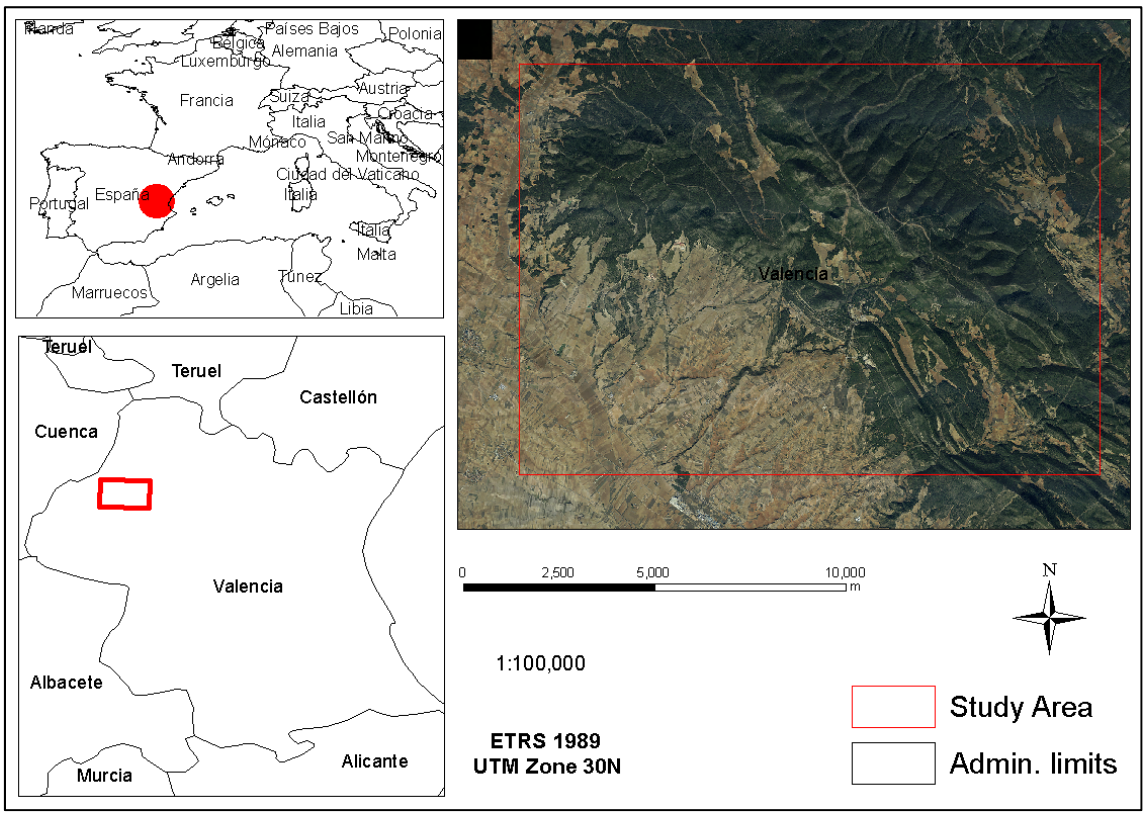

Figure 1. Allocation map of the study area

Climate can be considered as Mediterranean Pluviseasonal-Oceanic with the characteristic precipitation peaks in autumn and in spring highlighting a long drought season in summer. The mean precipitation in Utiel station was about 400 mm year in temperatures ranging -1.4ºC to 30.9ºC with an average on 12.2 ºC.

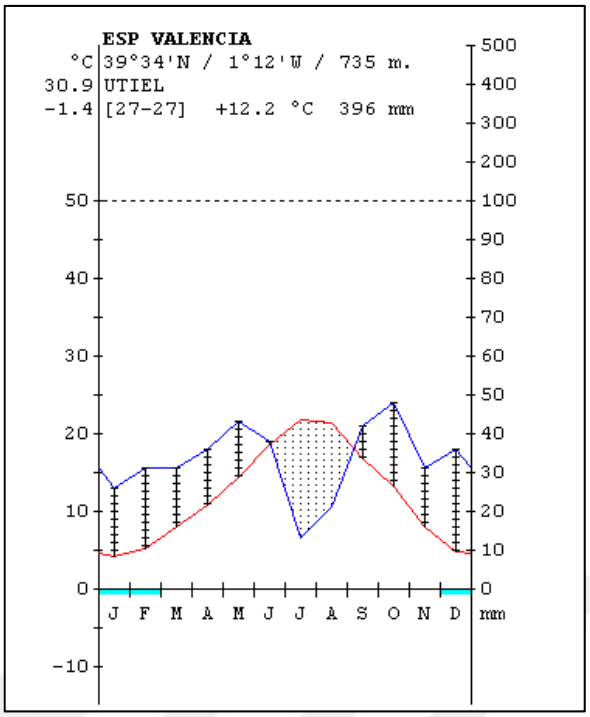

Figure 2.Diagrame Bioclimatic of Utiel. (1996-2009 S.Rivas-Martínez, Centro de Investigaciones Fitosociológicas, Madrid.)

The elevation ranges from 740m to 1304m with an average of 948m.

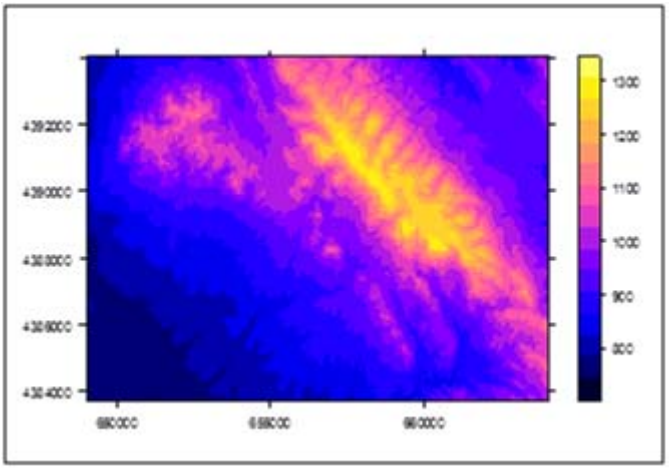

Figure 3. Elevation map of the study area (Elevation in meters).

In aspects map is showed for the study area. The prevalent aspect is 225º and the majority of the aspect in the South.

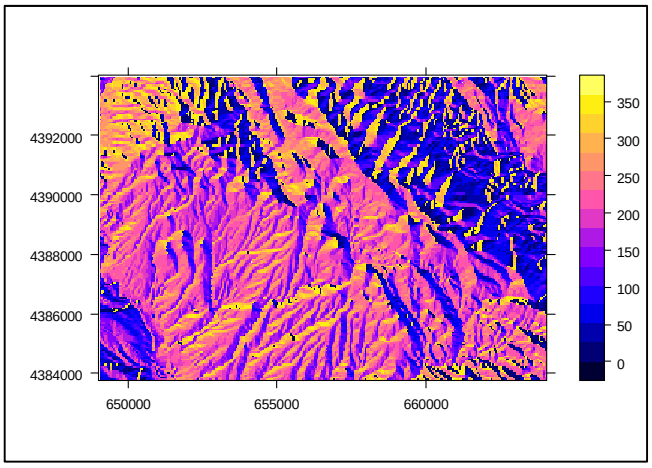

Figure 4. Aspect map of the study are

Figure 5 shows the slopes of the study area. The slopes range from 0 to 41.2% the mean slope is 8.34% but the 3rd quartile is 11.97%.

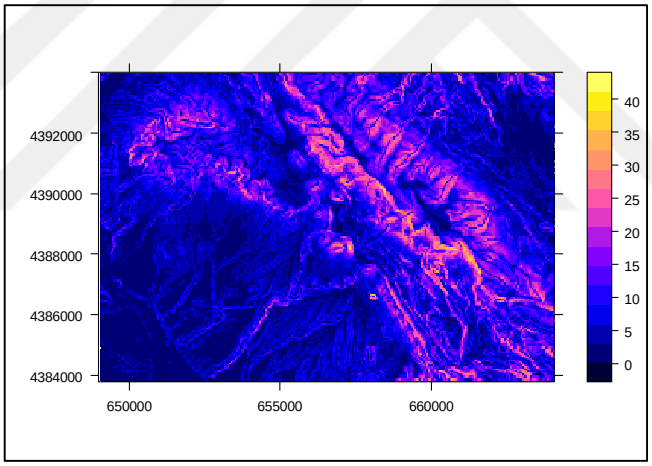

Figure 5. Slope map of the study area.

Bedrock is limestone in majority and prevalent soils are Leptosoles. The forest is characterized by sclerofilous vegetation mainly Aleppo pine (*Pinus halepensis* Miller) and Holm oak (*Quercus ilex* L.) and they appear also mixed forest. There exist orchards, olive trees and rain-fed crops such as vineyards.

The potential vegetation corresponds with the vegetation series *Bupleuro rigidi-Querceto rotundifoliae sigmetum.*

Legal limitations unravel the sectorial normative as the Forest Act in the Valencian Community in which clearcuttings are forbidden due to the potential erosion. Furthermore, regeneration method is the most important environmental constraint since the harvesting

method suitable for this species is the shelter wood method. The sequence of three different thinnings of different intensity does not leave the ground bare.

2.2. Data

The work reported in this master thesis was supported by data sensed remotely. Information from plot and LiDAR based field inventories served as reference for derivation of training areas, and in the stages that required accuracy assessment of estimated values. Satellite remotely sensed data and LiDAR based data was the base for fitting classification and regression models. Ancillary data used include aerial photography of 2010 and vector cartography.

2.2.1. Landsat

2.2.1.1. Selection of Images

Monitoring and analysis of forest dynamics require the acquisition of a time series satellite images that overlay the study area. Anniversary cloud-free images should be desirable in addition to those acquired in a stable phenological stage of vegetation. Atmospheric conditions not always are favorable to achieve high quality images. Besides to that, processing and analyzing anniversary images from the 70's decade until now implies a high computational effort. In this study, six summer Landsat images ranging from 1984 to 2014 were selected four from Landsat 5 sensor TM, one from Landsat 7 sensor ETM+ (Scan Line Correction on) and the most recent from Landsat 8 sensor OLI-TIRS. They were freely available from the United States Geological Survey (USGS) user interface (URL-1). Reflective bands were used in this work and excluded the thermal band from further analysis. They have a spatial resolution of 30m and are provided with Standard Terrain Correction (Level 1T) that ensures systematic radiometric and geometric accuracy. All of them are projected in the Universal Transverse Mercator (UTM), zone 30 North (datum WGS84) coordinate system.

For the study of vegetation changes in the Mediterranean area is suitable to select images from the summer period when the sun elevation in higher and, therefore, the

maximum radiance is received by the sensor. In addition, summer season is the time when the cloudiness is lower.

Table 1. Landsat imagery used in this work

Spacecraft	Sensor		Path	Row	Date		Sun elevation
LANDSAT_5	TM		199	33	8/20/1984		53.14
LANDSAT_5	TM		199	33	9/6/1990		47.77
LANDSAT_5	TM		199	32	7/24/2009		60.79
LANDSAT_5	TM		199	32	8/15/2011		56.47
LANDSAT_7	ETM		199	32	9/9/2000		49.78
LANDSAT_8	OLI_TIRS		199	32	8/7/2014		59.86

2.2.1.2. Image Pre-Processing

The computational effort and time of applying algorithms to a full image was reduced by cropping the original extent of the Landsat scene by a window that was better adapted to the study area.

Sun light energy cross the atmosphere, a part of it is absorbed by it or the earth surface and other part is reflected to the outer space crossing back the atmosphere. Also the earth surface emits a certain amount of energy but it is not of interest to the goal of this work. This energy is collected by the satellite sensor, transformed in Digital Numbers (DN) from 0 to 255 and stored in files that one can download from the USGS browser, as mentioned above.

The influence of the sun energy, the characteristics of the surface elements, the conditions and composition of the atmosphere crossed by the energy as well as the properties of the sensors are frequently the main causes of radiometric anomalies in the images. This may lead to errors when interpreting the real amount of energy emitted or reflected by the earth surface.

Radiometric calibration is a process to convert the Digital Numbers (DN) to at-satellite radiance, a radiometric quantity measured in $W/(m^2 \cdot sr \cdot \mu m)$ using the equation(3):

$$G = \frac{(Lmax - Lmin)}{(DNmax - DNmin)} \quad \textbf{1)}$$

$$B = Lmin - G \cdot DNmin \quad \textbf{2)}$$

$$L = G \cdot DN + B \quad \textbf{3)}$$

Where L is band-specific at-satellite radiance (W m^{-2} sr^{-1} μm^{-1}), *DN* is satellite quantized calibrated digital number, *B* is band-specific bias in *DN*, and *G* is band-specific gain ($m^2 \cdot sr \cdot \mu m \cdot W^{-1}$). *Lmax* is band-specific spectral radiance scaled to *DNmax* (W m^{-2} sr $^{-1}$ μm^{-1}), *Lmin* is band-specific spectral radiance scaled to DNmin(W m^{-2} sr $^{-1}$ μm^{-1}), *DNmax* is maximum quantized calibrated digital number (255), and *DNmin* is minimum-quantized calibrated digital number (0 for LPGS data, 1 for NLAPS data).

Then, to calculate at-sensor reflectance the equations are:

$$L_0 = \frac{[Esun \cdot sin(e)]}{\Pi \cdot d^2} \quad \textbf{4)}$$

$$\rho_{TOA} = \frac{L}{L_0} \quad \textbf{5)}$$

Where, d is the earth-sun distance in astronomical units, e is the solar elevation angle, E_{sun} is the mean solar exoatmospheric irradiance in W · m^{-2} · μm^{-1}, L_0 is the sun radiance in W m^{-2} sr^{-1} μm^{-1}, L is band-specific at-satellite radiance (W m^{-2} sr^{-1} μm^{-1}) and ρ_{TOA} is at-sensor or Top Of Atmosphere (TOA) reflectance.

2.2.1.3. Atmospheric Correction

The interaction between the electromagnetic radiation (EMR) and the atmosphere modifies by absorption and scattering the signal collected by the sensor. There are several approaches for the correction of these atmospheric effects that can be clustered in two main groups: Absolute and Relative algorithms.

Relative atmospheric correction algorithms require of the sensor spectral profile and the atmospheric conditions at the same time of the image acquisition.

The Dark Object Subtraction (DOS) method assumes that the darkest parts of an image (water, artificial structures) should be black if not for the effects of atmospheric scatter. Corrections make possible to use the black value from one band to correct the remaining bands.

The atmospheric correction method used in this work is DOS4. GRASS7 was used to transform the DN to at-surface reflectance with the *i.landsat.toar* command.

2.2.1.4. Topographic Correction

Various radiometric correction methods have been proposed to reduce topographic effects on remotely sensed images. The Minnaert correction method (Smith et al. 1980)adopts the bi-directional reflectance principles. In this correction, a measure of how close a surface is to the ideal diffuse reflector is introduced by the Minnaert constant. In Karathanassi et al. (2000) the classification based on the images generated by the Minnaert correction presented the highest overall accuracy and kappa coefficient for all scenes.

The topographic correction of the Landsat images was performed using the Landsat package in R with the command *minnaert*. (Lu et al. 2008) The Minnaert correction model can be expressed as Equation (6):

$$\mathrm{LH} = \mathrm{LT} \cos e \,/(\cos e \cos i)^k \quad \textbf{6)}$$

where LH is the equivalent reflectance on a flat surface with incident angle of zero, LT is the measured radiance in the remotely sensed data, k is a Minnaert constant, e is slope, and i is the solar incident angle in relation to the normal of a pixel. The cosine of the incident solar angle (cos i), referred to as illumination, is calculated using Equation (7):

$$\cos i = \cos\theta \cos e + \sin\theta \sin e \cos(\varphi_m - \varphi_s) \quad \textbf{7)}$$

where θ and φ_m are solar zenith angle and azimuth, and e and φ_s are slope and aspect of the terrain. In order to solve k, Equation (6) can be reorganized as Equation (8):

$$\log(L_T \cos e) = \log L_H + k \log(\cos e \cos i) \quad \textbf{8)}$$

Once atmospheric and topographic corrections were implemented on all images, the clouds and cloud-shadows were removed. To do this the *i.landsat.acca* the pre-processing stage was finished and the images were ready to be used in the production of derived products.

2.2.1.5. Vegetation Indexes

Reflectance of two or more bands may be combined in order to highlight a particular property of vegetation based mainly on the difference of reflectance in the Red and the NIR bands. One may find abundant literature regarding to VI's. Here, Normalized Difference Vegetation Index (NDVI), Enhanced Vegetation Index (EVI), Simple Vegetation Ratio (SR) were calculated as well as Tasseled Cap Transformation components (Brightness, Greenness, Wetness)

2.2.1.5.1. Normalized Difference Vegetation Index

Developed by Rouse et al. (1973), is one of the most widely used VI and can be defined as:

$$NDVI = \frac{NIR + R}{NIR - R} \quad \textbf{(9)}$$

Where NIR and R stand for the reflective values in the NIR and red bands for each pixel.

2.2.1.5.2. Enhanced Vegetation Index

The enhanced vegetation index (EVI) was developed to optimize the vegetation signal with improved sensitivity in high biomass regions and improved vegetation monitoring through a de-coupling of the canopy background signal and a reduction in atmosphere influences. The equation takes the form,

$$EVI = 2.5\,\frac{NIR - RED}{NIR + 6 + RED + 7.5\,BLUE + 1} \quad \textbf{10)}$$

where NIR, BLUE and RED are surface reflectance of near Infrared, blue and red bands, respectably (Huete et al. 2002)

2.2.1.5.3. Simple Vegetation Ratio

It is described as the ratio of light that is scattered in the NIR range to that which is absorbed in the red range.

$$\mathrm{SR} = \frac{\mathrm{NIR}}{\mathrm{R}ED} \quad \textbf{11)}$$

The range of values is from 0 to more than 30, where healthy vegetation generally falls between values of 2 to 8.

SR as well as NDVI and EVI were calculated using *i.vi* module in GRASS 7.

2.2.1.6. Tasseled Cap Transformation

The Tasseled Cap Transformation (TCT) was initially developed by Kauth and Thomas (1976) for crops and, then, broadly used in forest studies. The first three components of the TCT were named Wetness, Greenness and Brightness have received special attention for forest applications.

In Meddens et al. (2013) were used to detect bark beatle-caused mortality together with other vegetation indices.

They were computed using *i.tasscap* module in GRASS 7 from the Top Of Atmosphere (TOA) reflectance obtained with the *i.landsat.toar* module.

2.3. LiDAR Technology

LIDAR (Light Detection and Ranging) is a new accurate method to measure the topography of the Earth's surface. It consists of three different gears: A laser scanner installed in an aircraft that emits Laser pulses with a very high frequency that are reflected back to a receptor. The time that takes to reach an object or the ground and return back and the angle from nadir are used to determine the position of the reflecting surface.

The location of the instrument is captured by a Global Positioning System (GPS) and the Inertial Navigation System provides orientation characteristics. Then, x, y and z coordinates of the surface are given. In some cases the flux is partially reflected by two or more different objects located at different heights. This multiple returns may be collected by the sensor. The sensor also register the intensity, a spectral property of LiDAR data that measures the amount of energy backscattered from features on the Earth's surface.

2.3.1. LiDAR Data

Discrete LiDAR data for the study area were acquired on 2009 by the Instituto Geográfico Nacional (IGN). Nevertheless there existed a temporal bias between the forest management plan published, it was not considered important since, in this time interval, were not produced significant changes in the forest structure.

The sensor LiDAR used was Leica ALS 50. Data gathered by this sensor present the following specifications:

Table 2. Characteristics of LiDAR flight.

Density	0,5 hits · m^{-2}
Separation	1,41 m
Sensor	Leica ALS 50
FOV	50º
PRF	89.9
Frequency	33.2 Hz
Hv	2200

Speed	274 Km · h^{-1}
Overlapping	15%
Ellipsoid	ETRS89
Projection	UTM 30
Vertical accuracy	≤ 0.20 m RMSE
Horizontal accuracy	≤ 0.20 m RMSE

A total amount of 132 tiles of airborne LiDAR data, each with dimensions 2 x 2 km, were obtained from the IGN website (URL-2). Each tile is compressed in ".las" format, a

dense collection of georeferenced points with the following attributes: x coordinate, y coordinate, return height (z), return, and intensity. The raw tiles are delivered with a classification attribute that allows discriminating between the surface types that were hit. Although this classification could be useful, here was preferred to avoid it in our analysis.

The original information gathered by the sensor may contain errors since estrange elements such as birds or insects can interfere in the earth surface as well as its vegetal or anthropic cover. In addition, these returns generally differ considerably in height with other points of the ground and the rest of the objects and may cause variations in the data produced from the point clouds. On the other hand, the z coordinate is referred to an ellipsoid (in this case to ETRS89) and not the height over the ground that is the really necessary in order to perform the analysis of the variables.

2.3.2. LiDAR Data Processing

DEM (Digital Elevation Model) is a continuous mathematical model representing the shape of the surface, i.e. the elevation as function of the cartographic coordinates North-East or a function of latitude and longitude. There exist two different kinds of DEM: the digital surface model (DSM) that represents all objects over the Earth's surface including vegetation, buildings and so on; the digital terrain model (DTM) reproduces the bare Earth's surface.

Therefore, to correct these deficiencies one should realize the following processes:

- Extract the points due to noise ("Denoise").
- Classification of the points in ground and no ground
- Produce a Digital Terrain Model (DTM) and a Digital Surface Model (DSM)
- Normalization of the point-clouds to obtain height over the ground
- Extraction of the variables

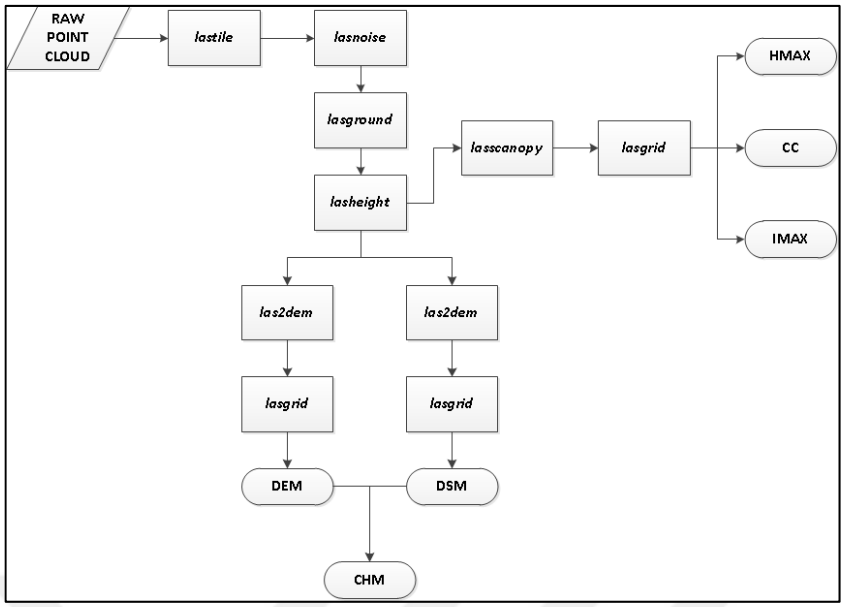

Figure 6. Lidar processing workflow diagram using *Lasstools***.**

LasTools is a new software suite for the operational processing of data from advanced airborne LIDAR sensor systems. LasTools provides the tools required to generate DSMs and DTMs from raw or basically preprocessed LIDAR data in a stand-alone application (Hug *et.* Al, 2012)

The initial 2 x 2 km tiles were split in 4 tiles of 1 x 1 km, thus, the computational time when applying the algorithms was dramatically reduced. Each of the resulting tiles had a buffer of 50m in each of its sides to avoid possible errors in the edge. At the end of the analysis this buffers were removed and all the tiles were merged.

2.3.2.1. Denoise

Lasnoise tool was used to find potential noise points. This tool tries to find points that have only few other points in their surrounding 4 m by 4 m by 4 m cube of cells with the cell the respective point falls into being in the center. Thus, the noise points are given the classification code 7 (low or high noise).

2.3.2.2. Ground and No-Ground Points

Lasground is a tool for bare-earth extraction: it classifies LiDAR points into ground points (class = 2) and non-ground points (class = 1). The functioning of this tool is based in the assumption that the last return is considered as ground while earlier returns are considered non-ground. In this step were ignored the points classified as noise points.

2.3.2.3. Height Normalization

Then we height-normalize the LiDAR using *lasheight*. As we know that there are no trees higher than 28 meters in this plot we drop all LiDAR points that are higher than 30 meters that may be bird hits or other noise.

2.3.2.4. LiDAR Derived Variables

A Canopy Height Model (CHM) is a raster representation of the tree canopy height. In the normalized tiles resulting from the last step there exist points that returned from trees but also from buildings, shrubs, scrubs and other features. The most typical approach to obtain the CHM is by the subtraction of the DTM to the DSM. One approach to generate the DTM is to create a digital elevation model (DEM) with the points classified as last returns. On the other hand, the DSM is performed on the same way but with the first returns. In this work was used the *las2dem* module to obtain DTM, DSM raster layers and with its difference, the CHM raster layer. Elevation as well as slope and aspect raster layers derived from the DTM were computed using R statistics software (R Development Core Team 2011).

On the other hand, with the height normalized tiles as input, the *lascanopy* tool was used to produce a Canopy Cover (CC) raster layer computing the average percent of surface covered by vegetation; a Maximum Height raster layer (HMAX), registering the first return with the maximum height on a pixel; and a Maximum Intensity raster layer (IMAX) with the maximum intensity within each pixel.

All raster layers were created with a 2m resolution on *.tif* format and later resampled (by averaging) to 30 x 30 m cell size in order to harmonize the resolution with the Landsat images.

2.3.3. Ancillary data

2.4. Datasets

Once processed Landsat images was obtained a dataset for each year including six reflective bands, three vegetation indices and three tasseled cap components. In addition, elevation, slope and aspect data derived from the DTM were included in the dataset of each year. Thus, the dataset is composed of 15 variables excluding for the year 2009 in which LiDAR-derived raster layers where included (table 3).

For the classification of the reference image (2009) CHM, HMAX, CC, and IMAX were additional predictor variables. Later was compared the accuracy of using Landsat only (LO), Landsat and Vegetation Index dataset (LV) and fusion of LVT with LiDAR derived-predictors (FUSION).

Table 3. Model names and predictor variables.

Dataset	Variables
LO	B1, B2, B3, B4 , B5, B7
LV	B1, B2, B3, B4 , B5, B7, NDVI, EVI, SR, BRIGHT, GREEN, WET
LT	B1, B2, B3, B4 , B5, B7, ELEV,ASPECT,SLOPE
LLI	B1, B2, B3, B4 , B5, B7, NDVI, EVI, SR, BRIGHT, GREEN, WET, CHM,CC,HMAX,IMAX
LVT	B1, B2, B3, B4 , B5, B7, NDVI, EVI, SR, BRIGHT, GREEN, WET, ELEV,ASPECT,SLOPE
FUSION	B1, B2, B3, B4 , B5, B7, NDVI, EVI, SR, BRIGHT, GREEN, WET, CHM,CC,HMAX, IMAX, ELEV,ASPECT,SLOPE

LO: Reflective bands Landsat.; LV: Reflective bands Landsat + Vegetation indices + Tasseled Cap components, LT: Reflective bands Landsat + Topographic variables; LLI: LV + LiDAR derived variables; LVT: LV + Topographic variables; FUSION: LTV + LiDAR derived variables

2.5. Training Areas

Training data are indispensable for both classification and predicting purposes. Training polygons or areas are the input for the classifier. It could be suitable to carefully collect class, height and other ground information *in situ* with a global positioning system (GPS) receiver. Unfortunately, it requires not only certain budget but also a considerable amount of time. Thus, this data gathering method was not adopted in this work. Instead of this, training areas were drawn taking advantage of the vegetation strata map as well as the forest stands map from the forest management plan published in 2011. These reference maps were georeferenced using ARCMAP 10 and were used to digitize the sample polygons in the training of the Random Forest model.

Aerial imagery taken in 2010 with 25 cm of resolution delivered by the IDEE was used verification of training area classes and to visually interpret the results of the classification for the years 2009 and 2011 assuming that there were not important variations in these years with respect to 2010.

A simple heuristic method is often used to determine the training sample size as at least 10-30 per class, where is the number of spectral wavebands or other discriminating features used in the classification (Foody, 2009). The description of the different land cover classes used in this thesis is shown in Table 4. Land cover types description.

Table 4. Land cover types description.

CLASS	**Description**
Man-made	Arable land, crops, orchard; Urban and artificial surfaces; roads.
Pine	Forest with Pine as dominant trees with more than 80% of presence.
Mixed	Forest with Pine or Oak as dominant trees with less than 80% of presence.
Oak	Forest with Oak as dominant trees with more than 80% of presence.
Shrubs	Natural or semi-natural grasslands; shrublands

The mean spectral response of each class is presented in Spectral signatures of classes are shown from Figure 8 to Figure 12.

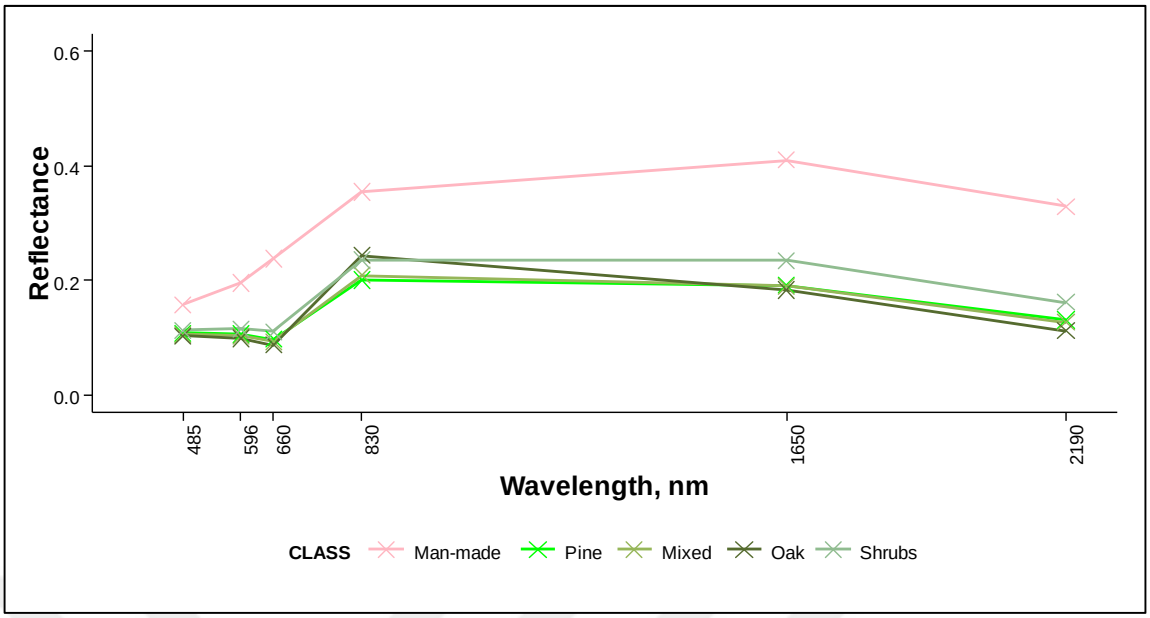

Figure 7. Mean values of the spectral response of the classes.

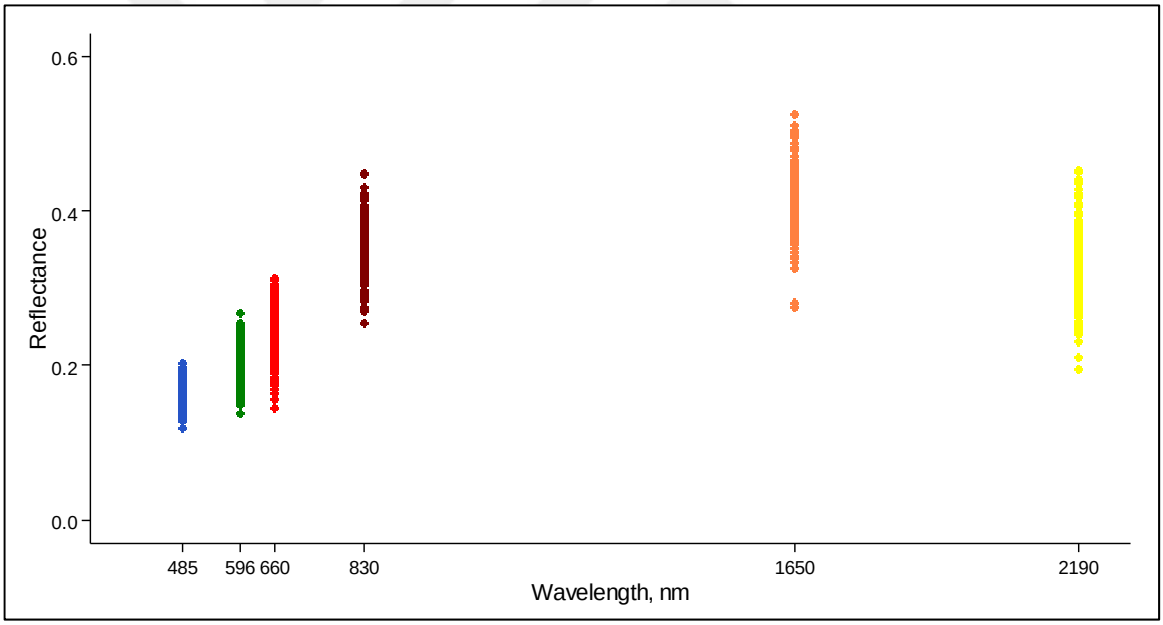

Figure 8. Spectral response for ‘Man-made’ class.

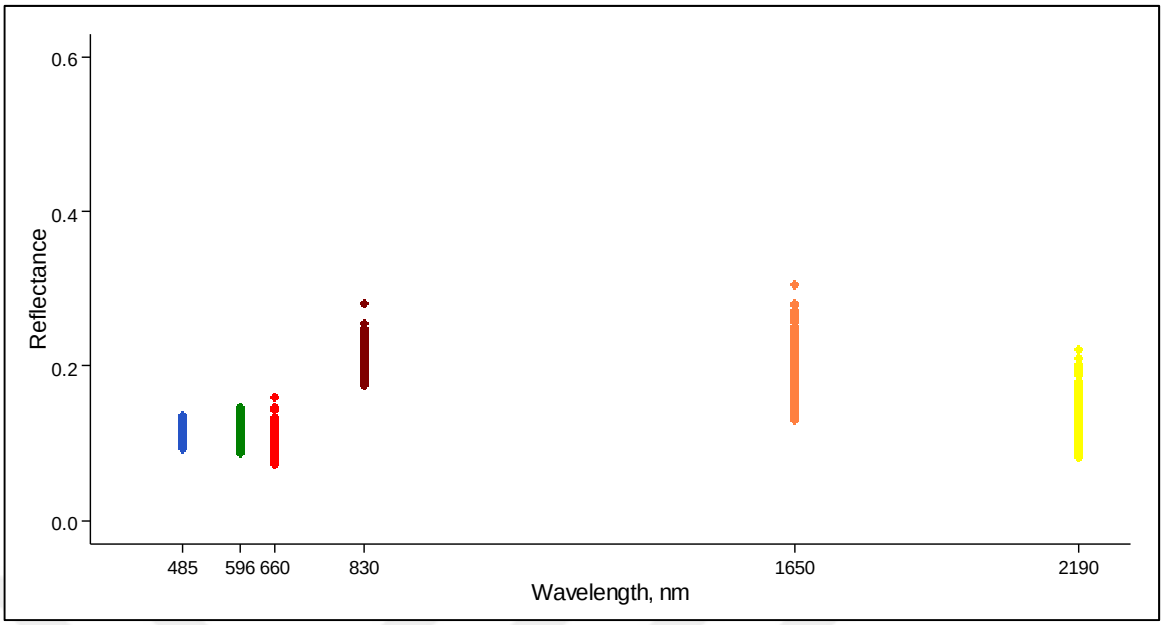

Figure 9. Spectral response for ‘Pine’ class.

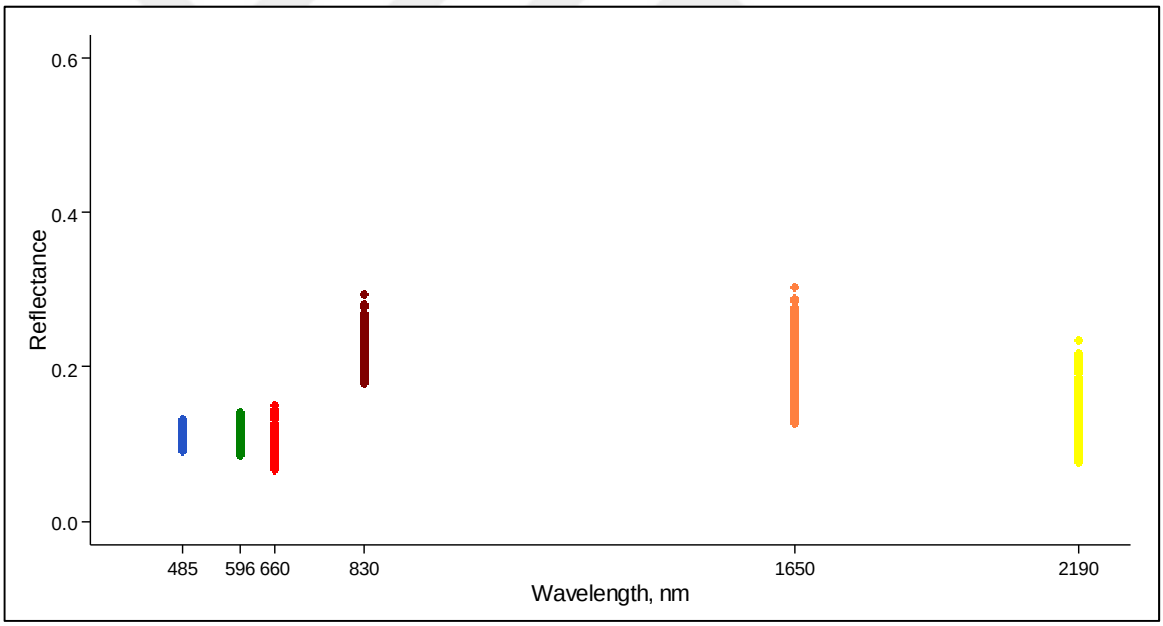

Figure 10. Spectral response for ‘Mixed’ class.

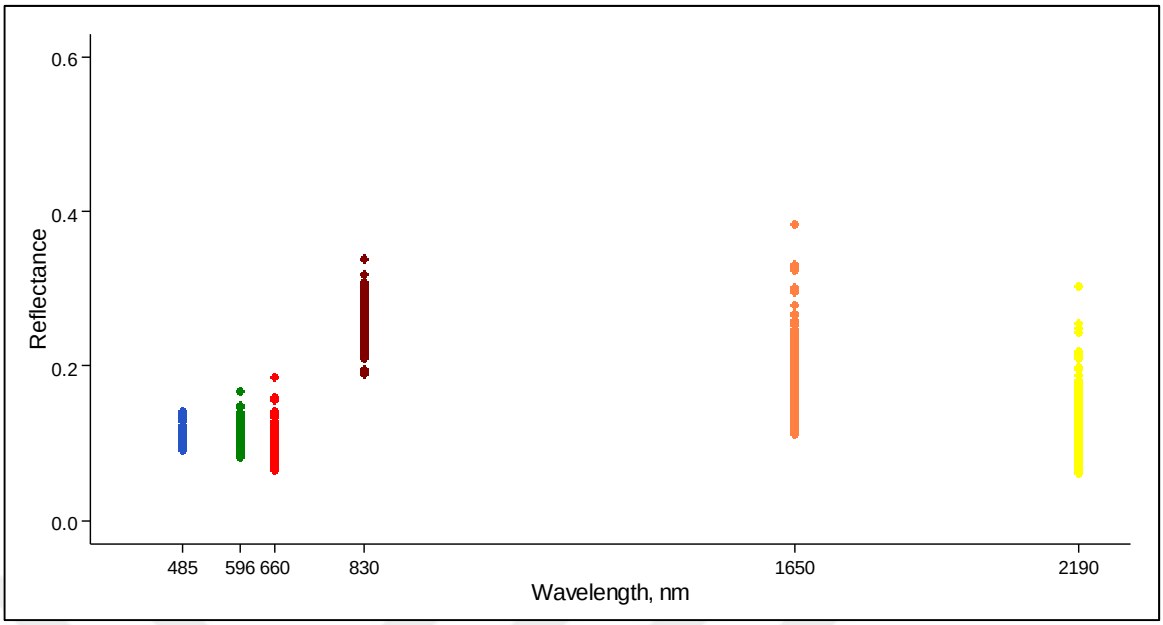

Figure 11. Spectral response for ‘Oak’ class

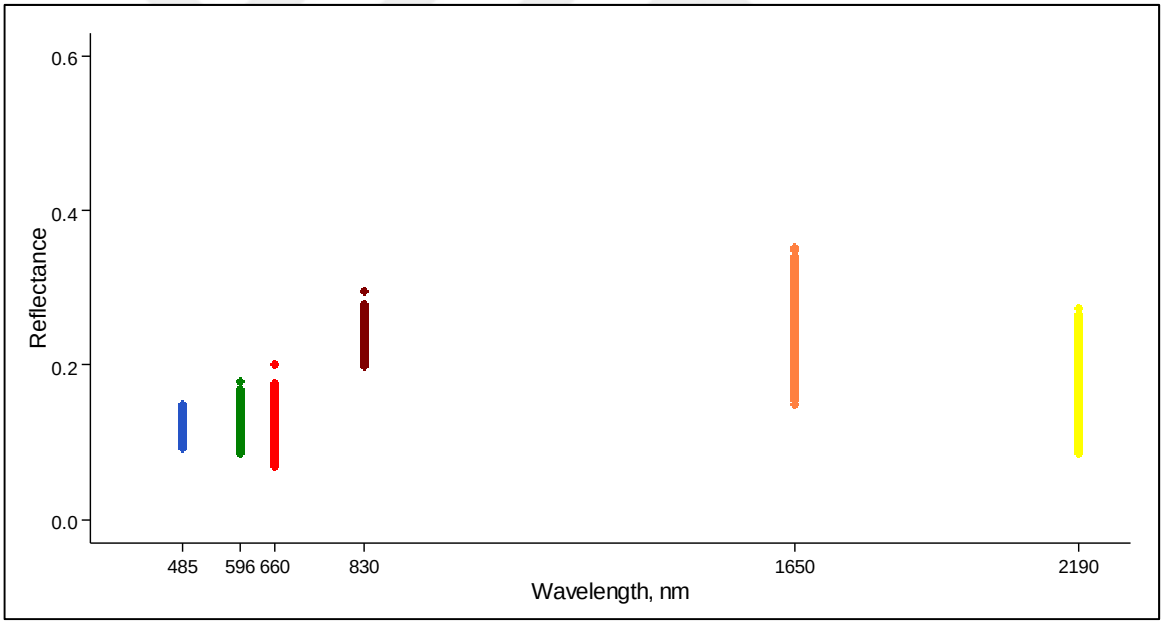

Figure 12. Spectral response for ‘Shrubs’ class.

2.6. Classification Algorithms

Identify to which category (or class) a new observation belongs is a statistics problem called classification. Thus, based on a training data containing information of observations whose class is known, one can achieve the objective of determining the class of each feature. According to (FAO, 1998) land cover and land use mapping is considered a supervised learning classification problem in which the response variable corresponds some biophysical properties of the earth surface such as dominant vegetation, soil composition, and so on in the presence, or absence, of human activities.

Classification algorithms are abundant in the literature and they are used for a large amount of problems. One of the most common techniques is the decision trees (Rokach 2016), predictive models that use a set of binary rules to calculate a target value. The basic decision tree induction algorithm constructs decision trees in a top-down recursive divide-and-conquer manner. In each iteration, the algorithm searches for the best partition of the data- set. Recall that many decision trees are univariate i.e. the dataset is split according to the value of a single attribute. Thus, in such cases, the algorithm needs to find the best splitting attribute. The selection of the most appropriate attribute is made according to certain splitting criteria, such as information gain or the Gini coefficient. All possible attributes are evaluated according to the splitting criterion and the best attribute is selected. After the selection of an appropriate split, each node further subdivides the training set into smaller subsets and the process continues in a recursive manner.

2.6.1. Random Forest

Breiman (2001) developed a classifier based in the combination of several decision trees. Random Forests is a classifier consisting of a collection of tree-structured classifiers $\{h(x,\theta_k), k = 1,...\}$ where the $\{ \theta_k \}$ are independent identically distributed random vectors and each tree casts a unit vote for the most popular class at input x. This technique examines a large ensemble of decision trees, by first generating a random sample of the original data with replacement (bootstrapping), and using a user-defined number of variables selected at random from all of the variables to determine node splitting. Multiple subsets of trees are built, and the support for the role of each variable in each decision is

noted. Finally, classification output is created based on a majority vote of the predictions from all individually trained trees, for regression the average of the results is used.

About 33% of the cases in the training dataset are left out to estimate the error rate, called Out Of Bag (OOB) data, and variable importance. Then, the OOB are used to validate the model and represents the average of the misclassification of all the trees. The number of trees should be enough to maintain the error rate stable (Horning 2010). The relative importance of a predictor variable may be evaluated.

The advantages of RF are the easy parametrization, since only the number of trees (ntree) and the number of variables to be randomly selected in each node (mtry); accuracy and variable importance are automatically generated; not very sensitive to outliers in training data; RF is able to deal with categorical data; and no need for pruning trees.

2.7. Accuracy Assessment

Training samples or training areas were drawn in ARCGIS v.10 taking as reference the vegetation strata map from the forest management plan and the aerial photograph from 2010.

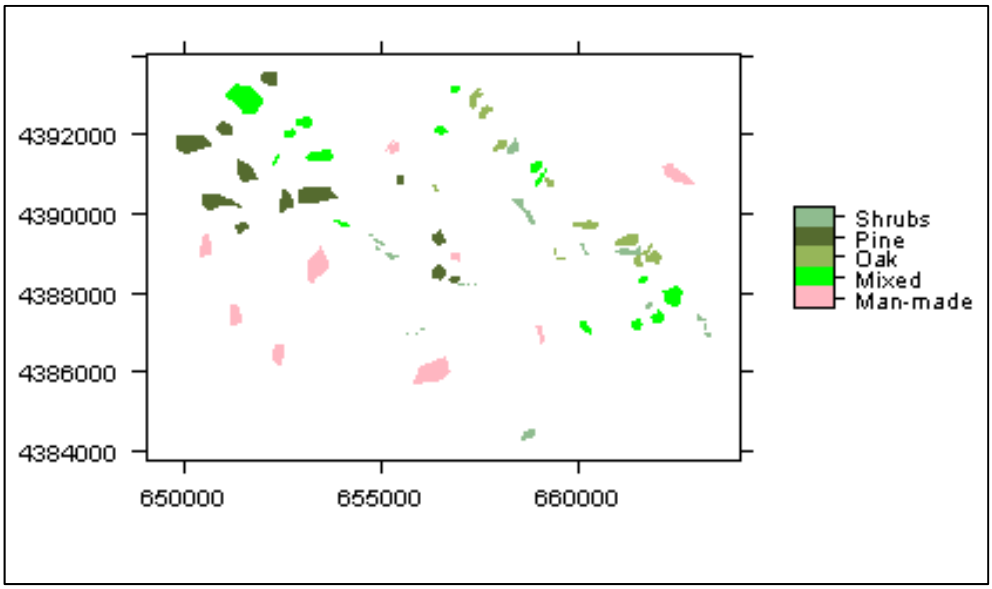

Figure 13. Trainning areas.

For classification each dataset was divided to 60% for training (training dataset) and 40% for validation or test dataset (TD). For regression each dataset was divided to 30% for training the model and 70%for validation.

RF performance in binary classification (forest-non-forest) as well as in multiclass was assessed in this work.

The output of the random forest consisted of OOB error rate and a confusion matrix for each classification RF. Then, with the predicted values obtained using test dataset as input, confusion matrix was attained. Producer's and User's accuracies were calculated as well as the overall accuracy for both, OOB and TD. (Thomlinson et al. 1999) set a target of an overall accuracy of 85% with no class less than 70% accurate.

2.7.1. Cohen Kappa Agreement ands Mcnemar's Test

The agreement of the classifications was analyzed by means of the Kappa agreement index (Cohen, 1960) and McNemar's test (McNemar, 1947) was used to find differences between classifications produced with the different RF models.

2.8. Landscape Analysis

The spatial structure and composition of the studied landscape were analyzed using a small number of metrics to evaluate patterns and processes as in Başkent & Kadioğullari (2007) and Martinez del Castillo et al. (2015). Binary and multiclass cover maps were used as input for the ClassStat command in the "SDMTools" package (Vanderwal et al. 2012) within the R statistics software. The output of this command is a data frame with class statistics based on statistics calculated by FRAGSTATS (Mcgarigal, 1994). In this study we analyzed percent of landscape (PL; percent of landscape), class area (CA; sum of the areas of all patches belonging to a given class, in map units), number of patches (NP), largest patch index (LPI; percentage of the landscape comprised by the largest patch), mean patch area (MPA; the average patch size within a particular class), patch density (PD; number of patches per 100ha), mean shape index (MSI: mean shape index), aggregation index (AI: computed simply as an area-weighted mean class aggregation index, where each class is weighted by its proportional area in the landscape) and patch

cohesion index (COHESION: measures the physical connectedness of the corresponding patch type)

Table 5. Landscape metrics assessed in this study, analysis level and landscape structure concept.

Index	Acronym	Analysis level	Landscape structure concept
Percentage of Landscape	PLAND	C	Fragmentation
Class area	CA	C	Fragmentation
Number of patches	NP	L/C	Fragmentation
Patch density (#/100 ha)	PD	L/C	Fragmentation
Largest patch index	LPI	L/C	Fragmentation
Patch Area (mean)	MPA	L/C	Fragmentation
Aggregation index	AI	C	Connectivity
Patch Cohesion Index	COHESION	C	Connectivity

2.9. Estimating CHM, HMAX and CC

RF models were developed using the 30% of the dataset as training samples. The models were validated with the rest 70% that was not used in the training of the models. R^2 and RMSE were reported. *Pseudo-*R^2 was calculated directly by the software R.

2.10. Software

This study was conducted using OPEN SOURCE software with the exception of the digitalization of training areas since the format *.ecw* was only compatible with the software ArcGIS.10.2 (ESRI 2013) and the format .laz that was with Lastools (Hug et al. 2012). The preprocessing of Landsat images was performed using GRASS 7 (Neteler, 2008) and R statistical.

The RF modeling was performed using the "random forest" package (Liaw, 2015) in R statistical language (R Development Core Team 2011). Landscape metrics were calculated using package "SDMTools". Other packages were used in this work such as

“rgdal” (Pebesma et al. 2012), “raster” (Hijmans et al. 2014), “ggplot2” (Wickham, 2009), “Landsat” (Goslee, 2011) and “irr” (Gamer et al. 2012).

3. RESULTS

This section provides all the results. The following sections present the classification results for the year 2009. Accuracy of the proposed random forests for classification was assessed using OOB error rate and error matrix, both, from the training dataset and from the test dataset. Importance of the variables was also analyzed. Categorical maps for the 1984, 1990, 2000, 2011 and 2014 were produced using the random forest that obtained the best accuracy considering the availability of the data.

3.1. Classification

3.1.1. Multiclass Classification Overall Accuracy Results

All the RF models presented a very good performance, having a glance to the OOB and to the test data accuracies, all of them exceeded of 85%. FUSION obtained the highest accuracy among all RF with and OOB of 95.37% and 95.16% in the TD while the highest error was registered by LV (13.59% and 14.64, in OOB and TD, respectively). The accuracy achieved LVT (94.51 and 94.58%) is similar to FUSION that demonstrates that in this work LiDAR did not improve in a considerably way the performance in the classification. In line with this, the addition of the LiDAR-derived features (LLI) to the model trained with LV (Landsat bands and Vegetation indices) only improved the performance accuracy 5.33% while LVT increased the accuracy about 10% with respect to LV. Thus, the addition of topographic information to the RF training dataset leads to a higher improvement in accuracy terms than the addition of LiDAR-derived features in the land cover classification in this work.

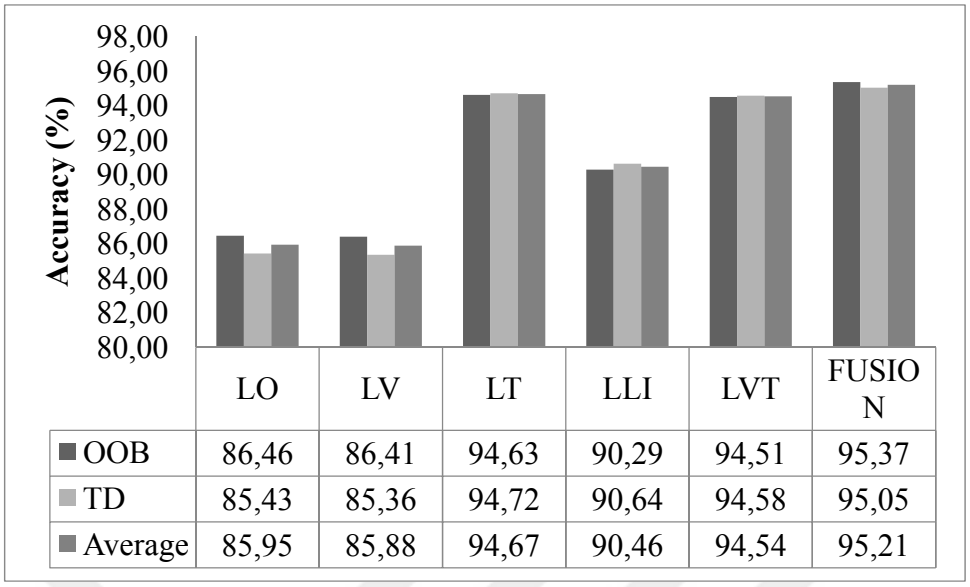

	LO	LV	LT	LLI	LVT	FUSION
OOB	86,46	86,41	94,63	90,29	94,51	95,37
TD	85,43	85,36	94,72	90,64	94,58	95,05
Average	85,95	85,88	94,67	90,46	94,54	95,21

Figure 14. Classification overall accuracies of the different RF models in OBB, TD and Average.

3.1.1.1. Kappa Test Results

Kappa analysis on the individual confusion matrices from each RF is presented in the Table 6. Similar results were obtained both, in the training level (OOB) and in the test level (TD). All models showed very strong agreement since all Kappa values surpassed 0.80. FUSION, LVT and LT achieved the highest Kappa values (0.94, 0.93 and 0.93, respectively) while LO and LV got the lowest results, both OOB and TD about 0.80.

Table 6. Kappa analysis based on OOB and Test Data (TD).

	LO		LV		LT		LLI		LVT		FUSION	
	OOB	TD	OOB	TD	OOB	TD	OOB	TD	OOB	TD	OOB	TD
Kappa	0.82	0.81	0.82	0.81	0.93	0.93	0.87	0.88	0.93	0.93	0.94	0.94

According to the results, the addition of topographical variables (LT and LVT) increased agreement greatly respects to LO and LV with a difference of the overall Kappa superior to 0.10. However, the addition of LiDAR-derived (LLI) variables presented a lower increase in agreement terms (0.05 and 0.07, OOB and TD, respectively). The improvement of the model performance due to the integration of LiDAR data with spectral and topographical data (FUSION) was only of 0.01 with respect to LVT but about 0.12 with respect to LO, in terms of Kappa.

3.1.1.2. User's and Producer's Accuracy Results

Average User's (UA) and Producer's (PA) accuracies of individual land cover type are presented in Table 7. All accuracies were higher of 75%, the lowest was 75.05% and the highest was 99.86%. Among all classes, Man-made class PA's and UA's were almost 100% in all cases. The PA's of 'Pine' were ranged from 85.49% to 95.20%. The PA's of 'Oak' were slightly lower to the 'Pine' ones ranging from 82.91% to 94.03. The 'Shrub' class PA achieved the widest range from 75.05% to 92.68% followed by the 'Mixed' class (76.24% to 94.03%). The highest class-specific PA's of all classes was generated by FUSION.

Regarding to UA's, 'Pine' ranged from 84.76% to 95.99%. The UA of 'Oak' was slightly lower ranging from 83.10% to 94.54%, the 'Mixed' class achieved 77.01% to 92.68% and the 'Shrub' class had the widest range from 76.05% to 92.52%. For 'Man-made', 'Pine' and 'Mixed' the highest UA was obtained using FUSION model. On the other hand, LT was more accurate when classifying 'Oak' and 'Shrubs' classes with 99.59% and 92.67% in UA, respectively.

Table 7. Average class-specific classification accuracies in percent. PA: Producer's Accuracy, UA: User's Accuracy.

CLASS	LO		LV		LT		LLI		LVT		FUSION	
	PA	UA	PA	UA	PA	UA	PA	UA	PA	UA	PA	UA
Man-made	99.68	99.29	99.27	99.48	99.80	99.29	99.32	99.71	99.79	99.36	99.86	99.82
Pine	85.49	84.76	86.63	85.96	94.49	95.09	91.03	91.11	95.10	94.94	95.20	95.99
Mixed	76.24	77.07	77.06	77.01	91.55	90.70	83.06	83.22	91.32	91.77	92.68	92.66
Oak	86.20	83.92	82.91	83.10	93.14	94.54	88.87	88.81	93.48	93.08	94.03	93.32
Shrubs	76.81	80.24	75.04	76.05	92.59	92.52	86.21	85.37	89.97	90.73	92.68	91.60

The improvement in the PA and the UA regarding to the addition of LiDAR and topographical variables to the reflective bands to train the model is evident in almost all the cases. It is possible to highlight that the addition of topographical variables improved considerably PA and UA for all classes in concordance with the overall accuracies since UA and PA are greater in LT with respect to LO, and in LVT than in LV. The

improvement in PA and in UA due to the incorporation of the LiDAR-derived variables was lower than when adding topographical variables. Nevertheless, the better performance was obtained integrating both, topographical and LiDAR-derived variables.

3.1.1.3. McNemar's Test Results

In general, McNemar's test results (Table 8) revealed that the classification carried out with LO, LV, LT, LLI and LVT were not statistically different since all p-values in pairwise analysis were greater than the significant level ($\alpha = 0.05$). Nevertheless, there was found that FUSION performed better than the other RF models excluding LT and LVT that performed equally. Thus, the cheaper and quicker model is LT.

Table 8. McNemar's test results for the TD.

	$\chi 2$	p-value
LO vs LV	6.947	0.7304
LO vs LT	12.5073	0.2525
LO vs LLI	8.6789	0.5628
LO vs LVT	10.1642	0.4262
LO vs FUSION	19.4892	0.03447
LV vs LT	4.535	0.92
LV vs LLI	7.8341	0.645
LV vs LVT	6.7991	0.7443
LV vs FUSION	20.2591	0.0269
LT vs LLI	7.8341	0.645
LT vs LVT	6.7991	0.7443
LT vs FUSION	12.3268	0.2638
LLI vs LVT	8.1393	0.6152
LLI vs FUSION	24.8752	0.005587
LVT vs FUSION	4.1292	0.9413

Taking into consideration the overall accuracies, the UA and the McNemar's test results, the model that better performed was FUSION and it was used to draw the land cover map of the year 2009. However, it was not possible to use this RF due to the lack of LiDAR data in the other years of the study. Hence, LT was used for the classification of the rest of the years since, having similar results than LVT in terms of OA, PA, UA, Kappa agreement index; it is the most simple of both.

3.1.1.4. Variable Importance Results

As mentioned in the random forest section, an interesting output from this algorithm is the variable importance In Table 9 are shown the variables used in each of the models ordered in descendent order of importance according the mean decrease in accuracy after the variable permutation. Thus, the most important variable across all the more accurate models (LT, LVT and FUSION) was ELEVATION followed by ASPECT. SLOPE also resulted important in LT and LVT but less important in FUSION. From the LiDAR-derived variables, CC as the most important ranking the first in LLI and the third in FUSION. CHM ranged the second in importance in LLI and the fourth in FUSION.

EVI resulted to be the most important of the vegetation indices in the most of the cases and GREEN was of the Tasseled Cap components. In the model only ith reflective bands (LO), B4, B1 and B3 were the three most important.

Table 9. Variable importance from each RF classification model. Note they are ordered from the most important (top) to the less important (bottom).

LO	LV	LT	LLI	LVT	FUSION
B4	GREEN	ELEVATION	CC	ELEVATION	ELEVATION
B1	B1	ASPECT	CHM	ASPECT	ASPECT
B3	B4	SLOPE	HMAX	SLOPE	CC
B7	EVI	B4	IMAX	B4	HMAX
B2	B3	B1	GREEN	EVI	CHM
B5	B5	B3	EVI	GREEN	IMAX
	B2	B5	B4	B5	EVI
	B7	B7	SR	B7	SLOPE
	WET	B2	NDVI	NDVI	GREEN
	SR		B1	SR	NDVI
	NDVI		BRIGHT	B3	B4
	BRIGHT		WET	B1	SR
			B7	WET	B5
			B5	BRIGHT	B1
			B3	B2	B3
			B2		BRIGHT
					WET

3.1.1.5. Visual Assessment

A qualitative comparison of the generated land cover maps is performed in this section. **Hata! Başvuru kaynağı bulunamadı.** represents the classification maps generated using the different random forest models. LO, LV and LLI generated most noisy maps with a high amount of isolated pixels. This drawback seems to be reduced by the addition of topographical data (LT, LVT and FUSION). However, some differences can be seen particularly in the classification of 'vegetated' classes due to the similarity between these classes in terms of spectral response (**Hata! Başvuru kaynağı bulunamadı.**).

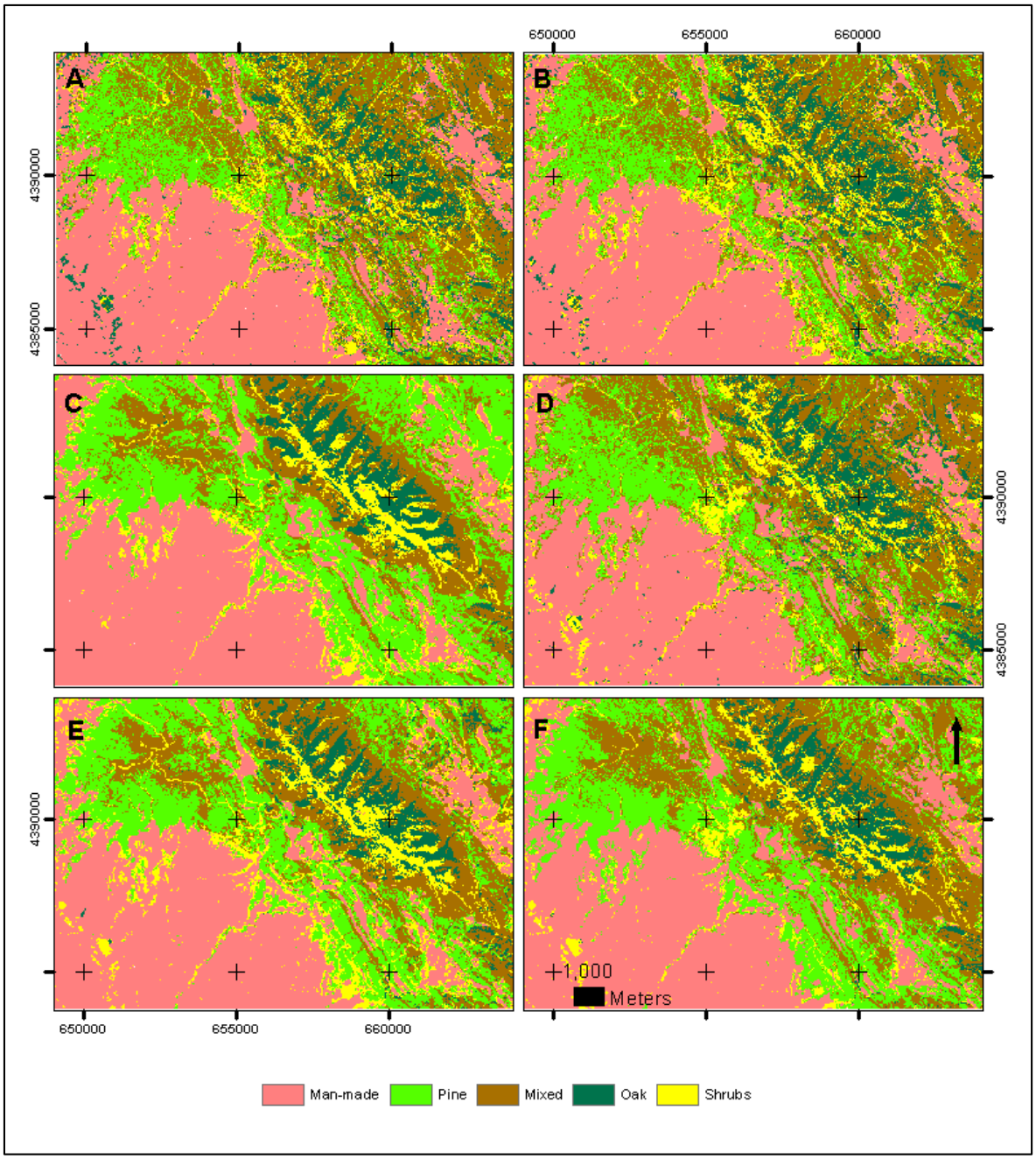

Figure 15. Classification maps achieved with all RF. A) LO, B) LV, C) LT, D) LLI, E) LVT and F) FUSION

3.1.1.6. Land Cover Mapping

Land cover maps for 1984, 1990, 2000, 2009, 2011 and 2014 are presented in Figure 16

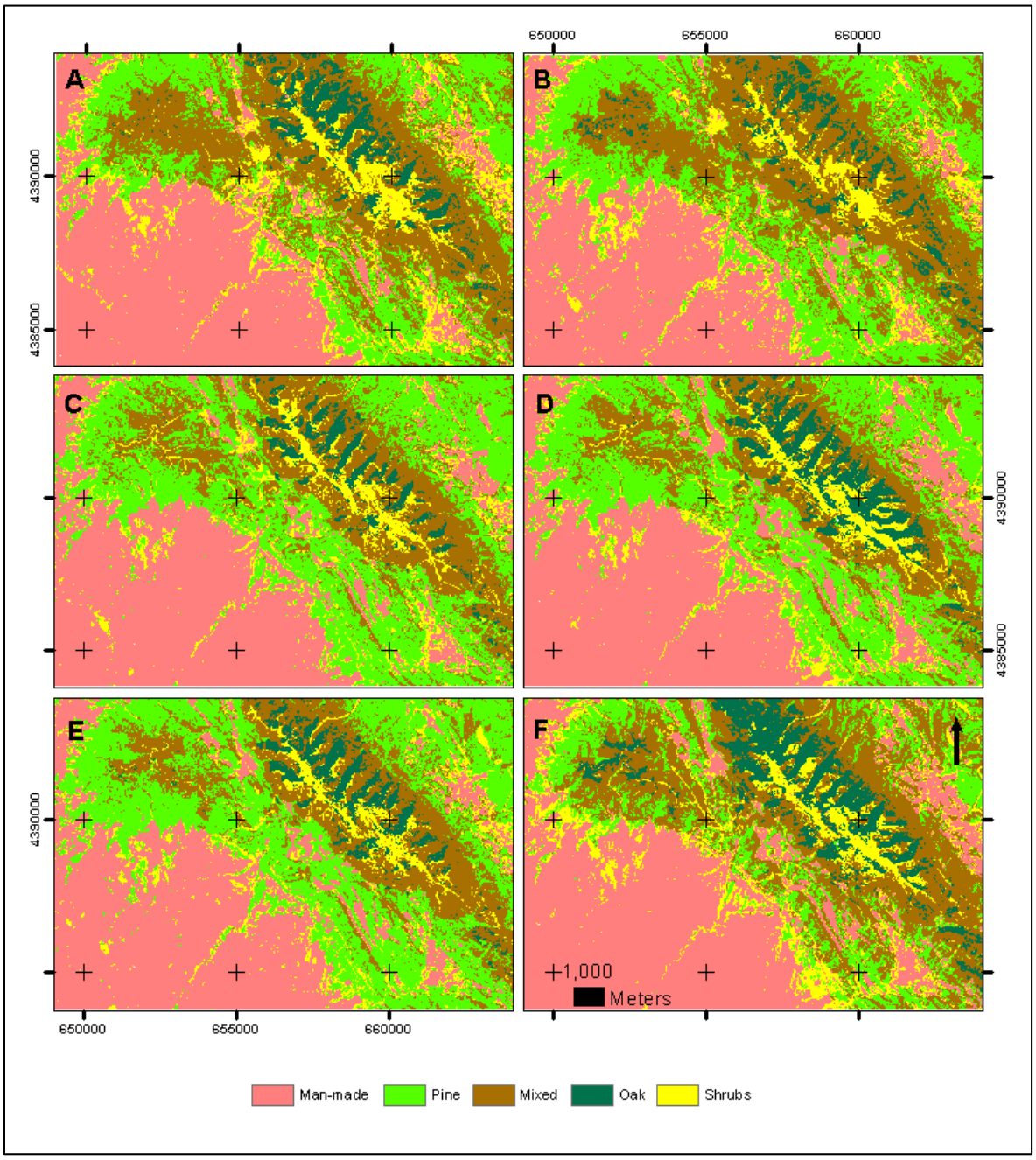

Figure 16. Land cover maps produced with LT model: A) 1984, B) 1990, C) 2000, D) 2009, E) 2011 and F) 2014.

3.1.2. Binary Classification

3.1.2.1. Classification Overall Accuracy Results

Figure 17 shows the overall accuracies in the binary classification. All models achieved better overall accuracies that in multiclass since all of them exceeded 95%. The highest OOB accuracy was achieved by FUSION and LT provided the highest TD accuracy. In average LT performed better in absolute terms but there were not found significant differences.

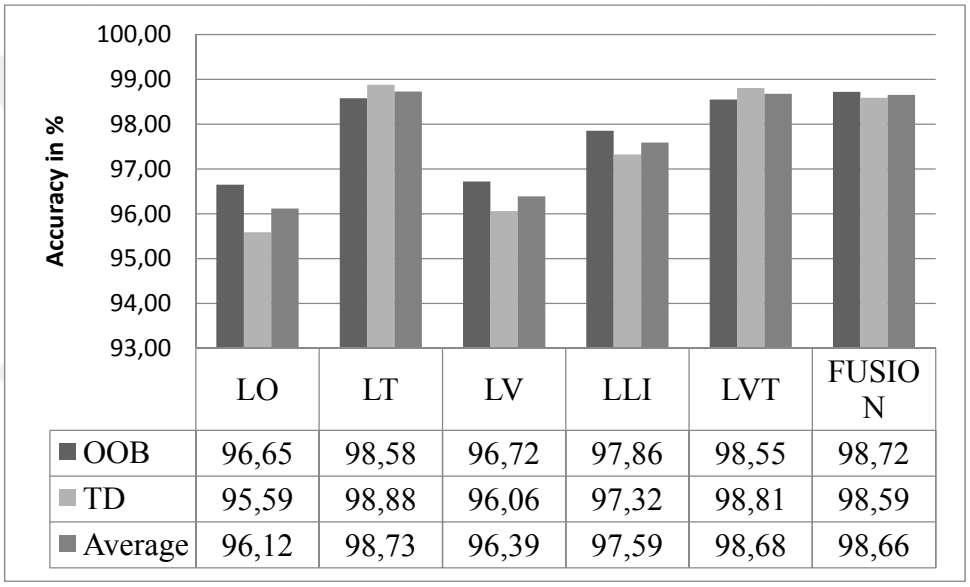

	LO	LT	LV	LLI	LVT	FUSION
OOB	96,65	98,58	96,72	97,86	98,55	98,72
TD	95,59	98,88	96,06	97,32	98,81	98,59
Average	96,12	98,73	96,39	97,59	98,68	98,66

Figure 17. Classification overall accuracies of the different RF models in OBB, TD and Average.

3.1.2.2. Kappa Test Results

With respect to the kappa agreement test all models obtained almost perfect agreement surpassing 0.9 with the exception of LO that achieved 0.898 in the test data (see Table 10). The best agreement was obtained by LT with a kappa index of 0.968 and 0.974, in OOB and TD, respectively. There were not significant differences between LT, LVT and FUSION.

Table 10. Kappa analysis based on OOB and TD.

	LO		LT		LV		LLI		LVT		FUSION	
	OB	D	OB	D	OB	D	OB	D	OB	D	OB	D
Kappa	.924	.898	.968	.974	.925	.909	.948	.94	.967	.973	.971	.968

3.1.2.3. User's and Producer's Accuracy Results

As occurs with the last sections, user's and producer's accuracies obtained here indicate that all the models perform almost perfectly since all of them exceed 90% in accuracy in both, forest and non-forest. According to Table 11, the highest UA was obtained by FUSION in detecting forest pixels but LT as better in separating non-forest, 99.06% and 98.15%, respectively. LVT obtained a better producer's accuracy in discriminating forest class (99.09%) and FUSION did in non-forest.

Table 11. Average class-specific classification accuracies in percent. PA: Producer's Accuracy, UA: User's Accuracy.

CLASS	LO		LT		LV		LLI		LVT		FUSION	
	PA	UA	PA	UA	PA	UA	PA	UA	PA	UA	PA	UA
Forest	97.72	97.64	97.83	99.00	97.82	96.87	98.28	98.16	99.09	98.96	98.95	99.06
Non-forest	92.78	97.56	97.93	98.15	93.42	95.34	96.15	96.39	97.84	98.10	98.05	97.81

3.1.2.4. McNemar's Test Results

According to results for the McNemar's test presented in Table 12, there were not found any difference between the binary classification obtained by the use of any of the models since *p-values* were higher than 0.05 and none of the values of the statistic χ^2 was higher than 3.84. Therefore, one can conclude that the use of the different variables studied in this work did not have impact in the binary classification in a significance level of 0.05.

Table 12. McNemar's test results for the TD

	χ^2	p-value
LO vs LV	0.1026	0.7488
LO vs LT	2.3486	0.1254
LO vs LLI	1.6569	0.198
LO vs LVT	2.4381	0.1184
LO vs FUSION	2.8174	0.09325
LV vs LT	1.7604	0.1846
LV vs LLI	0.9901	0.3197
LV vs LVT	1.9205	0.1658
LV vs FUSION	2.1635	0.1413
LT vs LLI	0.0533	0.8174
LT vs LVT	0	1
LT vs FUSION	0.0238	0.8774
LLI vs LVT	0.0548	0.8149
LLI vs FUSION	0.4571	0.499
LVT vs FUSION	0.025	0.8744

3.1.2.5. Variable Importance

The most important of the variables in the LO and LV model is B5. From the Landsat reflective bands, B4 is of relative importance in all models. Regarding the addition of vegetation indices, EVI and GREEN ranked the most important features in almost all the models they appear

The most important variable across LT, LVT and FUSION models was ASPECT followed by ELEVATION, conversely to the importance in multiclass classification. SLOPE also resulted important in LT and LVT but less important in FUSION. From the LiDAR-derived variables, CC as the most important ranking the first in LLI and FUSION. CHM ranged the second in importance in LLI and the fifth in FUSION.

Table 13.Variable importance from each RF model. Note they are ordered from the most important (top) to the less important (bottom).

LO	LV	LT	LLI	LVT	FUSION
B5	B5	ASPECT	CC	ASPECT	CC
B3	B4	ELEVATION	CHM	ELEVATION	ASPECT
B4	GREEN	SLOPE	B2	SLOPE	ELEVATION
B7	EVI	B5	HMAX	B4	HMAX
B1	B7	B4	IMAX	B5	CHM
B2	WET	B7	B3	EVI	SLOPE
	B3	B2	B4	GREEN	B4
	B2	B3	B5	B7	EVI
	BRIGHT	B1	B7	NDVI	WET
	NDVI		B1	SR	B2
	SR			BRIGHT	BRIGHT
	B1			WET	B5
				B2	B7
				B3	NDVI
				B1	B3
					GREEN
					SR
					IMAX
					B1

3.1.2.6. Visual assessment

A qualitative comparison of the generated land cover maps is performed in this section. **Hata! Başvuru kaynağı bulunamadı.** represents the classification maps generated using the different random forest models. LO, LV and LLI generated the most noisy. This drawback seems to be reduced by the addition of topographical data (LT, LVT and FUSION).

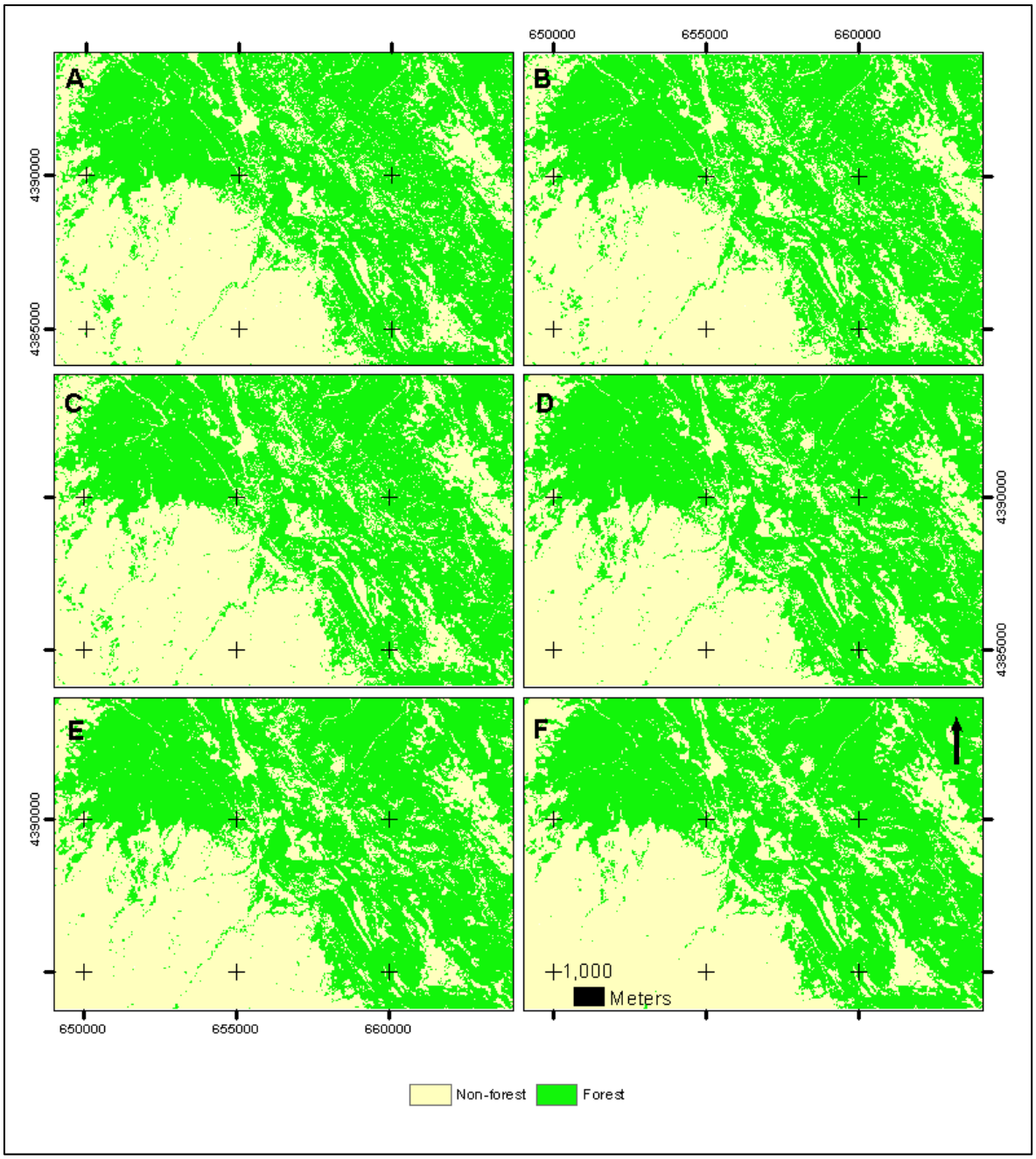

Figure 18. Binary classification maps achieved with RF models. A) LO, B) LV, C) LT, D) LLI, E) LVT and F) FUSION

3.1.2.7. Binary Classification mapping

The analysis realized of the models i.e. accuracy assessment, kappa test, McNemar's test in order to support the decision of which model use for the spatial distribution of Forested- Non-forested areas. None of the models tested here presented significant

differences regarding to the others. Facing this situation here was selected LT as long as this was the simplest and cheapest model.

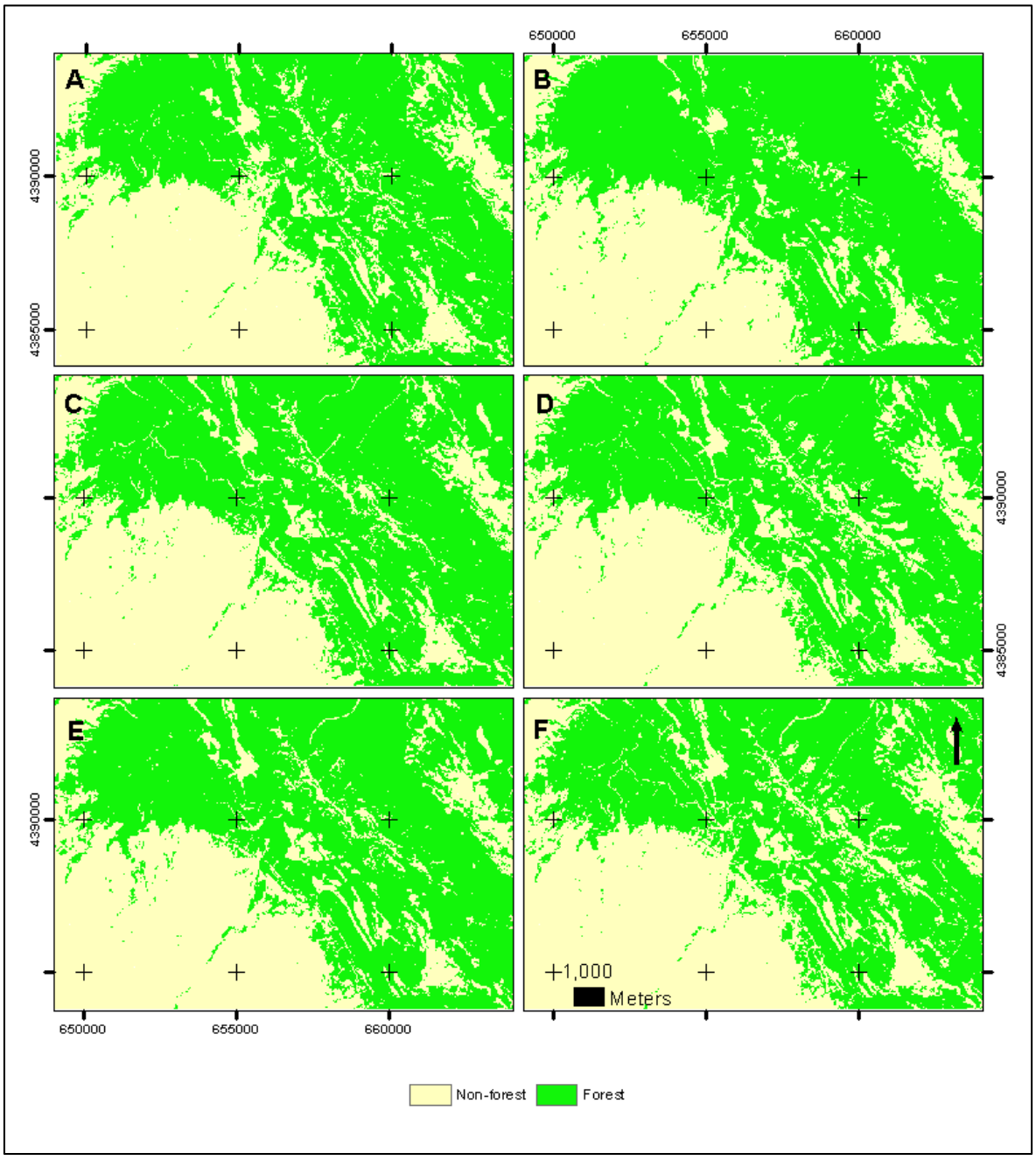

Figure 19. Binary classification produced with LT model: A) 1984, B) 1990, C) 2000, D) 2009, E) 2011 and F) 2014.

3.2. Land Cover Dynamics Analysis

Forest cover dynamics was explored by means of different non-redundant landscape metrics regarding not only to landscape level but also to class level or even both. These metrics were selected in order to assess both composition and structure temporal changes.

Forest landscape *composition* was assessed by means of the area covered by each class. Percent of landscape (PLAND) provides a more relative insight that the absolute class area (CA).

Landscape *structure* was quantified by means of patch-based metrics, shape-based metrics, size-based metrics and dispersion metrics.

Concerning to the patch-based metrics here were analyzed the number of patches (PN) and patch density (PD). In order to examine the size and shape of patches, the largest patch index (LPI), mean patch area (MPA) and mean patch size index (MSI) whilst dispersion was studied considering patch cohesion index (COHESION) and aggregation index (AGGREGATION).

3.2.1. Composition

3.2.2. Class Area

Result showed that forest area fell only slightly from 8269 ha (53.9% of the landscape) in 1984 to 8045.4 ha (52.5%) in 2014 during a 30 year period (Table 14). This reduction was uneven within the period since the landscape underwent sub-periods when the amount of forested area increased (1984-1990) with a maximum in 1990 of 9192 ha (60%). Pine forest increased from the beginning of the period occupying 3010.1 ha (19.6%) until 2011 when it extended 4956.7 ha (32.3%) and later decreased dramatically to 2138.7 ha (14%) in 2014. These differences may be explained by the use of different sensors. Nevertheless this trend was opposite regarding to mixed forest class that underwent a negative trend until 2011 but recovering in 2014 when as reached a similar level than in the first year of study 4234.7 ha (27.6%). Besides to this, pure oak forest had a slowly but positive tendency reaching at the end of the period about 1340 ha.

On the other hand, shrublands were reduced from 1907 ha to 1371 ha in 1984 and 2011 respectively but in the last period as recovered reaching 1834 ha. Man-made class

behaved more stable ranging from 4799.5 ha (31.3%) in 1990 to 5779.4 ha (37.7%) in 2014.

Table 14. Results of class area in ha. (Percent of landscape in %)

Cover type	CA (PLAND)					
	1984	1990	2000	2009	2011	2014
Forest	8269(53.9)	9192(60.0)	8746.2(57.1)	8265(53.9)	8848.7(57.7)	8045.4(52.5)
Non-forest	7060.(46.1)	6137(40.0)	6582.8(42.9)	7061.9(46.1)	6480.3(42.3)	7282.7(47.5)
Total Binary	15329(100)	15329(100)	15329.0(100)	15326.9(100)	15329(100)	15328.1(100)
Man-made	5363.2(35)	4799.5(31.3)	5364.4(35.0)	5716(37.3)	5218.3(34)	5779.4(37.7)
Mixed forest	4282.1(27.9)	4574.8(29.8)	3299.5(21.5)	2834.9(18.5)	3106.6(20.3)	4234.7(27.6)
Oak forest	766.4(5.0)	603.5(3.9)	493(3.2)	888.1(5.8)	676.2(4.4)	1340.9(8.7)
Pine forest	3010.1(19.6)	3773.9(24.6)	4778(31.2)	4411.3(28.8)	4956.7(32.3)	2138.7(14.0)
Shrublands	1907.3(12.4)	1577.3(10.3)	1394.1(9.1)	1476.6(9.6)	1371.2(8.9)	1834.4(12.0)
Total Multiclas	15329(100)	15329(100)	15329(100)	15326.9(100)	15329(100)	15328.1(100)

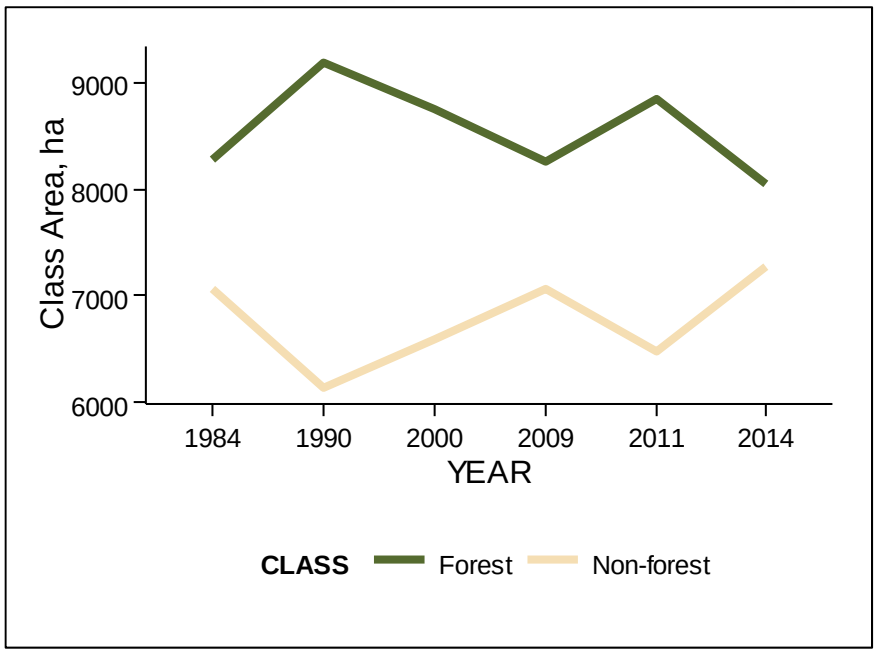

Figure 20. Evolution of the CA in the binary classification during the study period

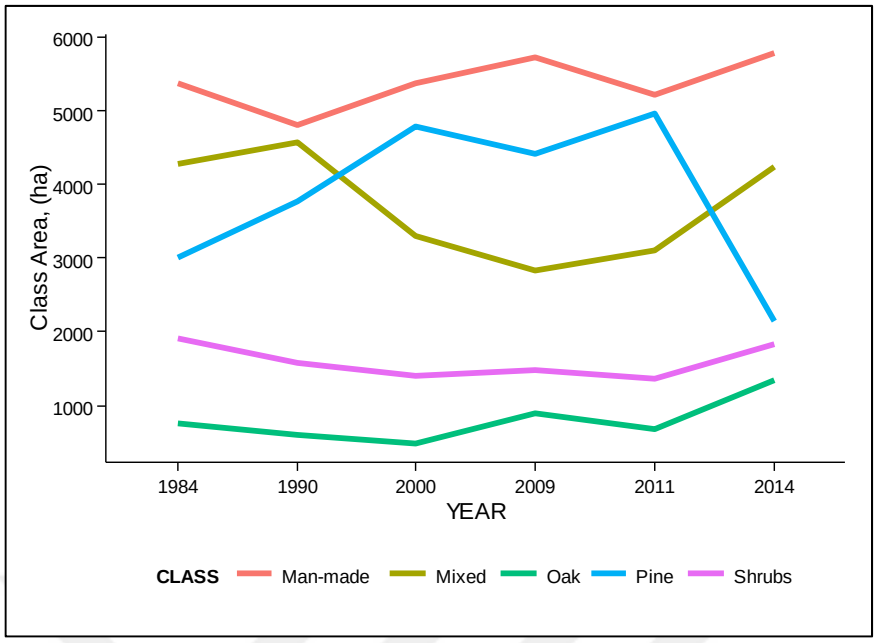

Figure 21. Evolution of the CA in the multiclass classification during the study period

3.2.3. Number of Patches

Having into account the binary classification, the overall number of patches increased from 934 to 1034, in 1984 to 2014 respectively. Both, forest and non-forest patches rose in number within the three decades period. But this fact was not constant in the study period. In the multi-class classification this trend can be also observed. Pine patches rose from 964 in 1984 to 1284 in 2014 although the tendency as negative until 2011 reaching only 665 patches and three years after nearly doubled. However, mixed forest's trend was found completely opposite to pine forest. Oak forest underwent a slightly fluctuation within the study period reaching about 363 patches in 2014, about 30 more patches (10%). The number of patches of shrublands class also increased slightly from 1644 in 1984 to 2138 in 2000 but was reduced to1870 in 2014.

Table 15. NP in the study period

Cover type	NP					
	1984	1990	2000	2009	2011	2014
Forest	263	256	265	278	246	318
Non-forest	671	430	631	601	523	716
Total binary	934	686	896	879	769	1034
Man-made	437	380	392	290	342	384
Mixed forest	1108	1140	1284	1321	1336	976
Oak forest	331	376	315	286	372	363
Pine forest	964	869	651	743	665	1284
Shrublands	1644	1753	2138	1995	2005	1870
Total multiclass	4484	4518	4780	4635	4720	4877

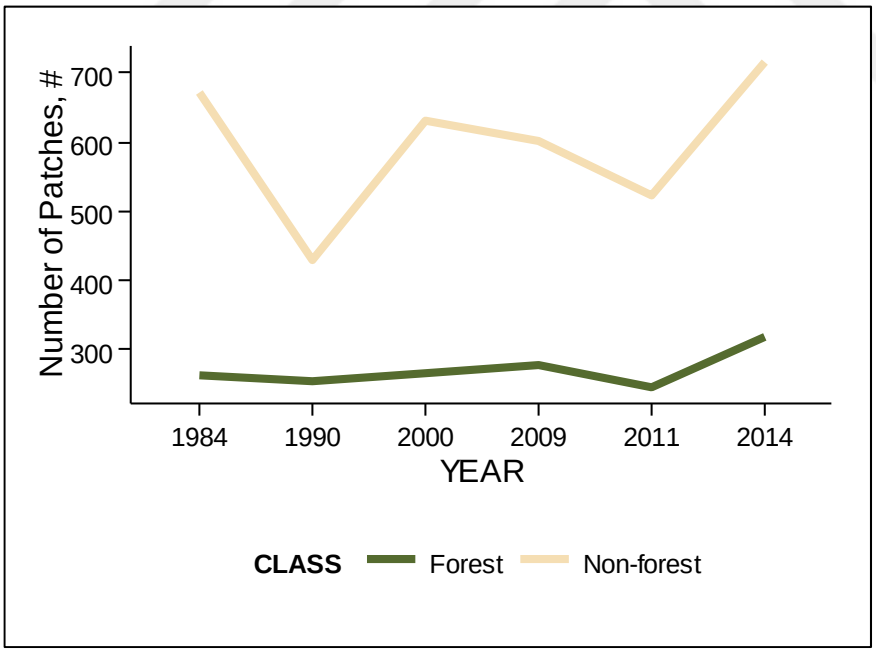

Figure 22. Evolution of the NP in the binary classification during the study period

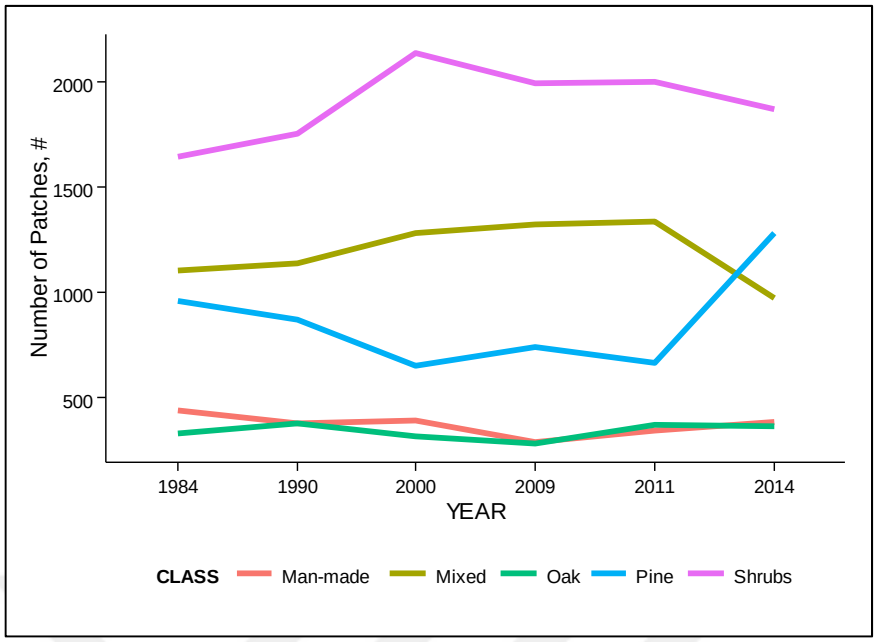

Figure 23. Evolution of the NP in the multiclass classification during the study period

3.2.4. Patch Density

Although the overall landscape patch density registered a slight increase of 10 % concerning the extremes of the study period, forest patch density as maintained until 2011 and in the last year augmented about 20% as well as Non-forest patch density. Pine forest patch density was reduced from 6.3 patches / 100 ha in the eighties to 4.3 patches / 100 ha in 2011 although in 2014 increased to 8.4 patches / 100 ha. Oak forest did not suffered significant variation in its patch density during all the period of study while mixed forest increased until 2011 and after as reduced to 6.4 patches / 100 ha in 2014. Pine forest patch density decreased from 6.3 patches / 100 ha in 1984 to 4.3 patches / 100 ha in 2011 and then doubled in 2014 until reach 8.4 patches / 100 ha. Shrublands patch density increased until 2000 and after as reduced to 12.2 patches / 100 ha.

Table 16. PD in the study period

Cover type	PD					
	1984	1990	2000	2009	2011	2014
Forest	1.7	1.7	1.7	1.8	1.6	2.1
Non-forest	4.4	2.8	4.1	3.9	3.4	4.7
Total binary	6.1	4.5	5.8	5.7	5.0	6.7
Man-made	2.9	2.5	2.6	1.9	2.2	2.5
Mixed forest	7.2	7.4	8.4	8.6	8.7	6.4
Oak forest	2.2	2.5	2.1	1.9	2.4	2.4
Pine forest	6.3	5.7	4.2	4.8	4.3	8.4
Shrublands	10.7	11.4	13.9	13.0	13.1	12.2
Total multiclass	29.3	29.5	31.2	30.2	30.8	31.8

If total landscape area is held constant, then patch density and number of patches convey the same information.

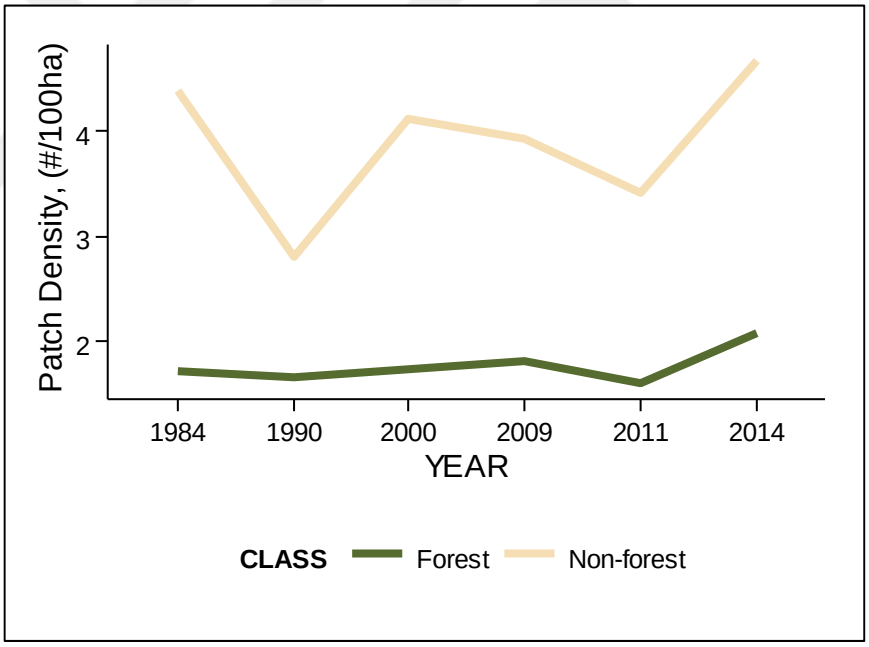

Figure 24, Evolution of the PD in the binary classification during the study period

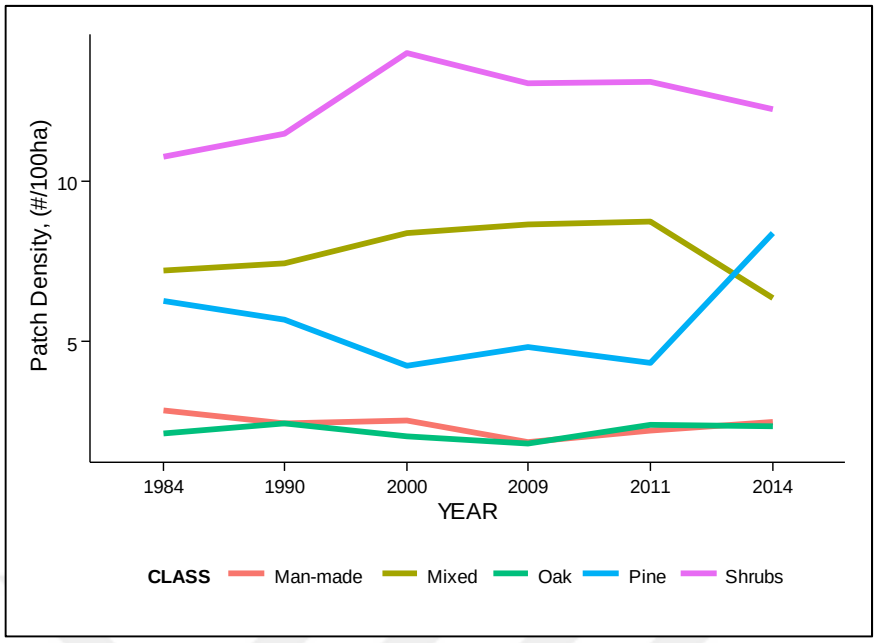

Figure 25. Evolution of the PD in the multiclass classification during the study period

3.2.5. Largest Patch Index

The largest patch index resulted to be a metric quite stable in this landscape and did not suffered important variations during the years of the study. It is possible to highlight that the largest patch of Man-made class was expanded about 29% of the landscape. Mixed forest LPI increased until 1990, decreased until 2009 and subsequently increased in 2014 to 12%. Pine LPI grew during the first years of study until 2011 when accounted with 22% of the territory studied and in 2014 dramatically shrank to 2%. The rest of land cover classes maintained the value of this metric over the time.

Table 17. LPI in the study period

Cover type	LPI					
	1984	1990	2000	2009	2011	2014
Forest	0.5	0.6	0.6	0.5	0.6	0.5
Non-forest	0.3	0.3	0.3	0.3	0.3	0.3
Total	0.9	0.9	0.9	0.8	0.9	0.8
Man-made	0.29	0.27	0.29	0.29	0.28	0.29
Mixed forest	0.16	0.24	0.13	0.07	0.10	0.12
Oak forest	0.02	0.01	0.01	0.02	0.02	0.03
Pine forest	0.05	0.08	0.18	0.18	0.22	0.02
Shrublands	0.02	0.01	0.02	0.03	0.01	0.02
Total	0.5	0.6	0.6	0.6	0.6	0.5

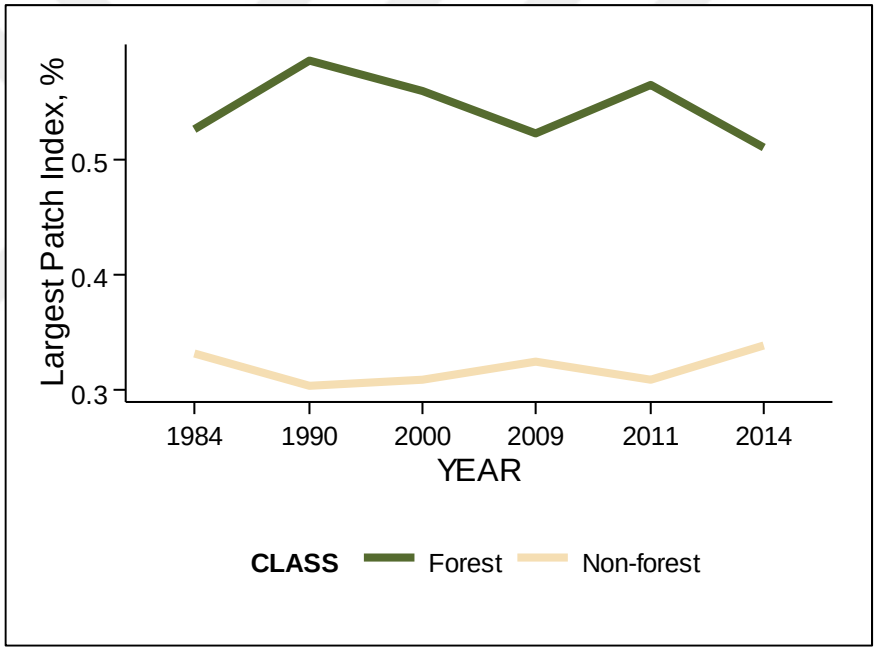

Figure 26. Evolution of the LPI in the binary classification during the study period

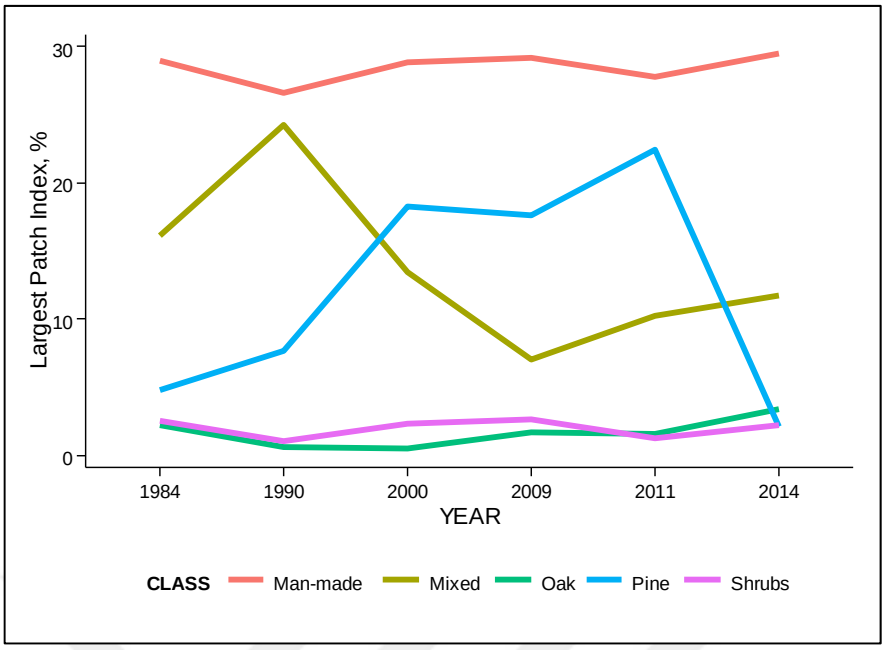

Figure 27. Evolution of the LPI in the multiclass classification during the study period

3.2.6. Mean Patch Area

Forest MPA resulted to grow during the 80's, decreased until 2009, increased again in 2011 until 36 ha and decreased in 2014 reaching 25.3 ha. Non-forest MPA suffered important variations during the study period ranging from 10.5 ha in 1984 to 14.3 ha in 1990. Forest MPA was 31.4 ha in 1984 and thirty years later descended to 25.3 ha. In the multi-class classification 'man-made' MPA increased from 1984 (12.3 ha) until 2009 (19.7 ha) but in the following five years decreased to 15.1 ha. Pine MPA increased from 3.1 ha to 7.5 ha, in 1984 and 2011, respectively, and suddenly was reduced to 1.7 ha. Oak MPA underwent an increase from 2.3 ha to 3.7, in 1984 and 2014. Mixed forest MPA increased slightly from 3.9 ha in the beginning of the period until 4.3 ha in 2014 while Shrublands MPA decreased slightly in 0.2 ha in the same period.

Table 18. MPA in the study period. (in ha)

Cover type	MPA					
	1984	1990	2000	2009	2011	2014
Forest	31.4	35.9	33.0	29.7	36.0	25.3
Non-forest	10.5	14.3	10.4	11.8	12.4	10.2
Total	42.0	50.2	43.4	41.5	48.4	35.5
Man-made	12.3	12.6	13.7	19.7	15.3	15.1
Mixed forest	3.9	4.0	2.6	2.1	2.3	4.3
Oak forest	2.3	1.6	1.6	3.1	1.8	3.7
Pine forest	3.1	4.3	7.3	5.9	7.5	1.7
Shrublands	1.2	0.9	0.7	0.7	0.7	1.0
Total	22.7	23.5	25.8	31.6	27.5	25.7

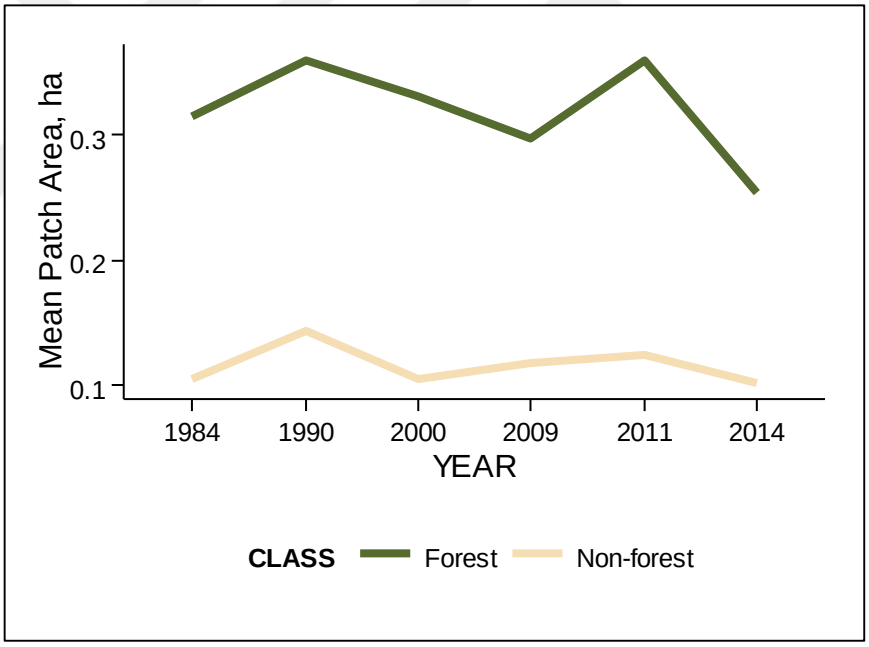

Figure 28. Evolution of the MPA in the binary classification during the study period.

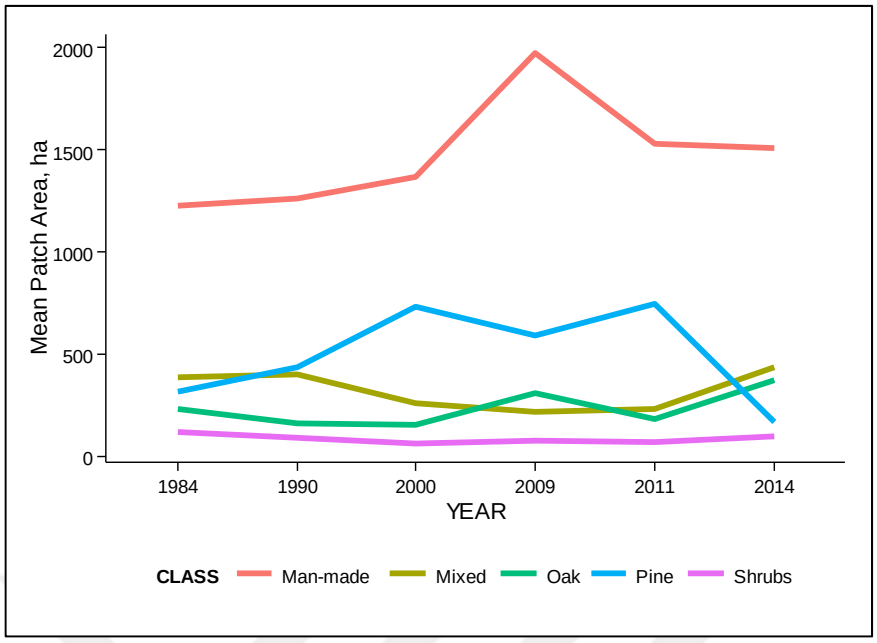

Figure 29. Evolution of MPA in the multiclass classification during the study period.

3.2.7. Mean Shape Index

Mean shape index was a very stable landscape metrics since changes in absolute terms never have exceed 0.06 and the maximum variation of MSI in percent was about 2.5 %.

Table 19. MSI in the study period.

Cover type	MSI					
	1984	1990	2000	2009	2011	2014
Forest	1.28	1.27	1.25	1.28	1.31	1.26
Non-forest	1.34	1.37	1.35	1.32	1.37	1.31
Total binary	2.62	2.64	2.6	2.61	2.69	2.57
Man-made	1.33	1.31	1.32	1.39	1.37	1.36
Mixed forest	1.33	1.28	1.26	1.25	1.27	1.32
Oak forest	1.3	1.37	1.25	1.29	1.23	1.32
Pine forest	1.34	1.3	1.29	1.28	1.27	1.36
Shrublands	1.34	1.31	1.24	1.26	1.27	1.32
Total multiclass	6.65	6.57	6.36	6.48	6.42	6.68

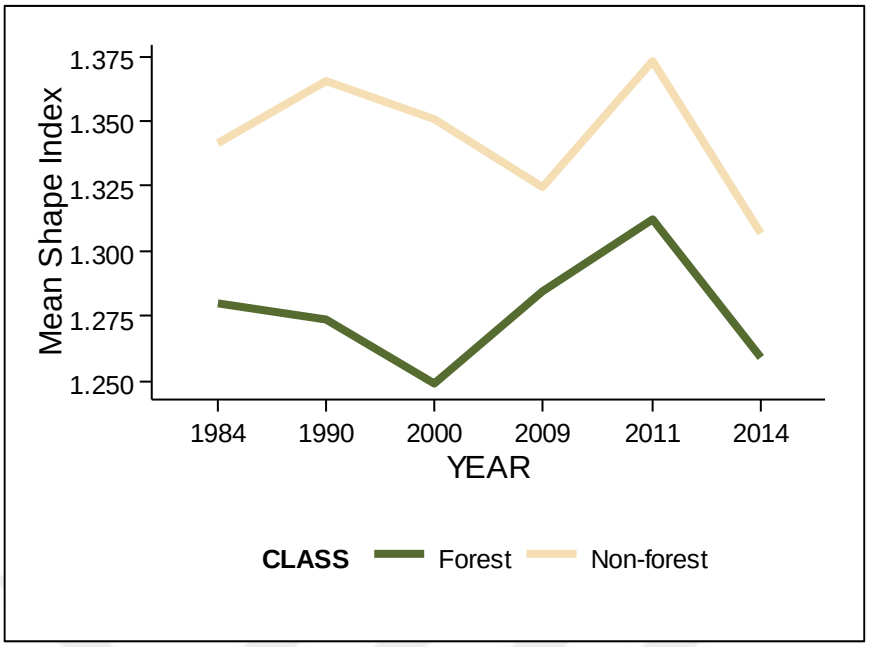

Figure 30. Evolution of MSI in the binary classification during the study period

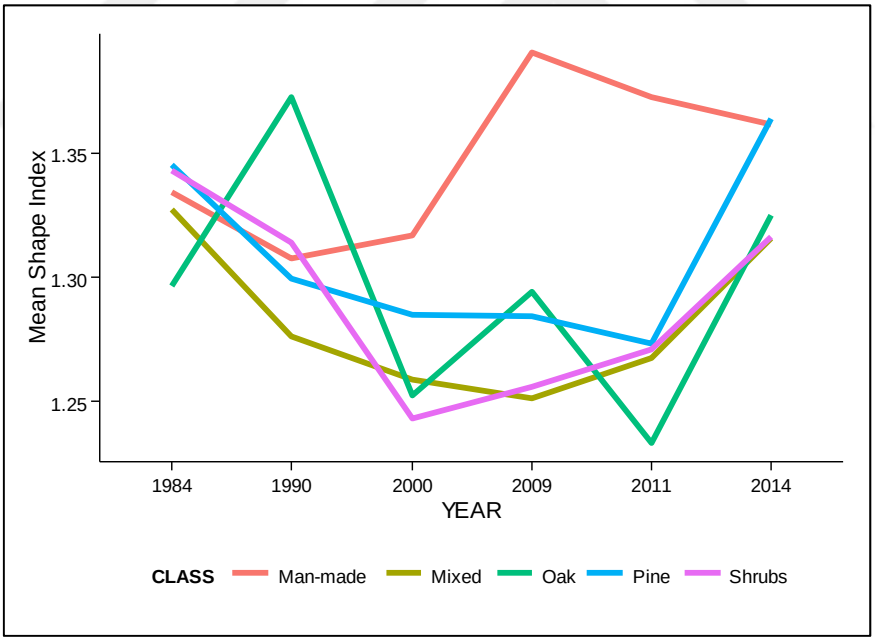

Figure 31. Evolution of MSI in the multiclass classification during the study period

3.2.8. Cohesion

As it was the case with MSI, COHESION showed not relevant variations over the whole period of study.

Table 20. COHESION in the study period.

Cover type	COHESION					
	1984	1990	2000	2009	2011	2014
Forest	9.9	9.9	9.9	9.9	9.9	9.9
Non-forest	9.9	9.9	9.9	9.9	9.9	9.9
Total binary	19.9	19.9	19.9	19.9	19.9	19.9
Man-made	9.9	9.9	9.9	9.9	9.9	9.9
Mixed forest	9.9	9.9	9.9	9.8	9.9	9.9
Oak forest	9.7	9.3	9.4	9.7	9.6	9.8
Pine forest	9.8	9.9	9.9	9.9	9.9	9.6
Shrublands	9.6	9.4	9.6	9.7	9.4	9.6
Total multiclass	49	48.4	48.7	49	48.8	48.7

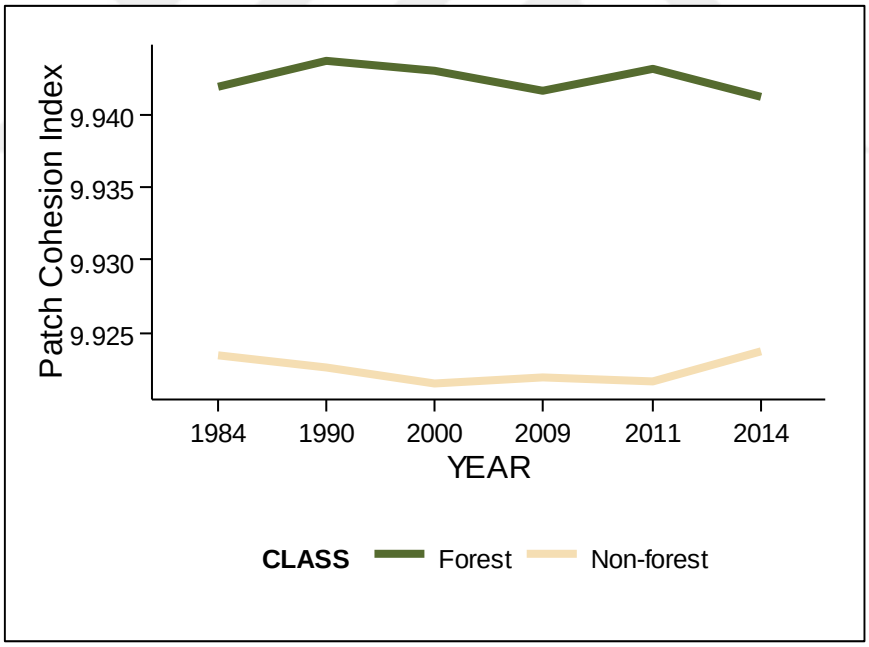

Figure 32. Evolution of AI in the binary classification during the period.

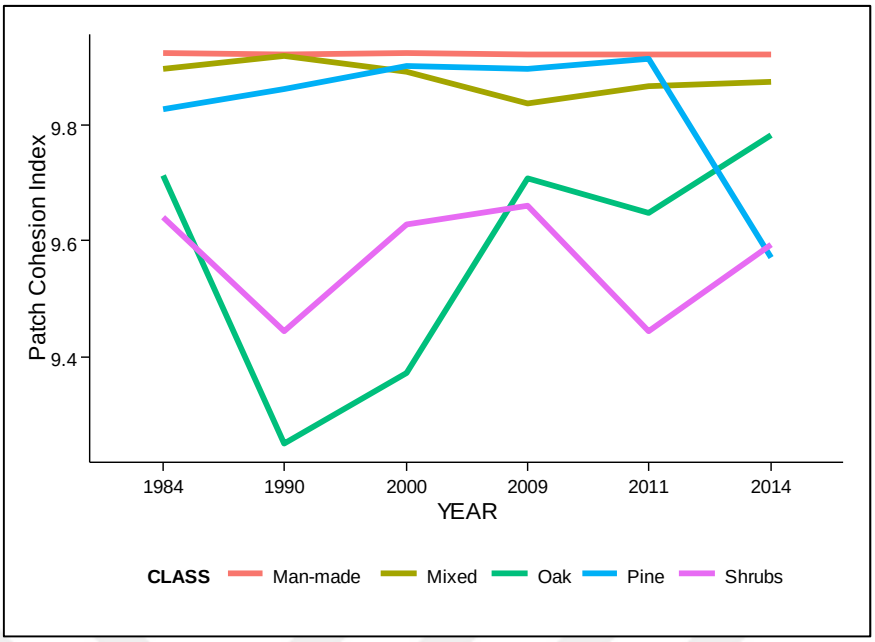

Figure 33. Evolution of COHESION in the multiclass classification during the period.

3.2.9. Aggregation

In Table 21. Aggregation index in the study period.are presented the results of the Aggregation index for the study area in the study period. It is possible to highlight the reduction of the pine AI in about 10% but in contrast the slightly increase of oak AI.

Table 21. Aggregation index in the study period.

Cover type	AGREGATION					
	1984	1990	2000	2009	2011	2014
Forest	93.7	95.7	94.4	93.7	94.7	92.6
Non-forest	92.6	93.5	92.4	92.6	92.7	91.8
Total binary	186.4	189.3	186.8	186.4	187.3	184.4
Man-made	93.3	92.5	93.6	93.8	93	93.2
Mixed forest	78.7	80.7	76.7	74.7	76.2	79
Oak forest	76.7	67.6	73.5	79.9	74.9	81.3
Pine forest	76.1	79.4	82.6	82.3	83.6	68.2
Shrublands	60.9	57.6	53.7	56.2	53	59.4
Total multiclass	385.7	377.7	380	387.1	380.7	381.1

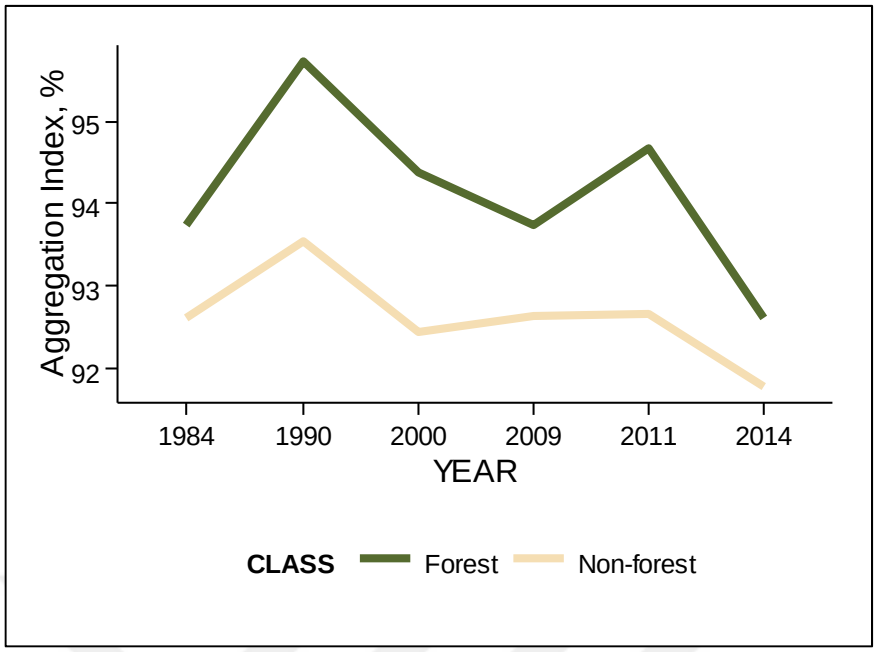

Figure 34.Evolution of AI in the binary classification during the period.

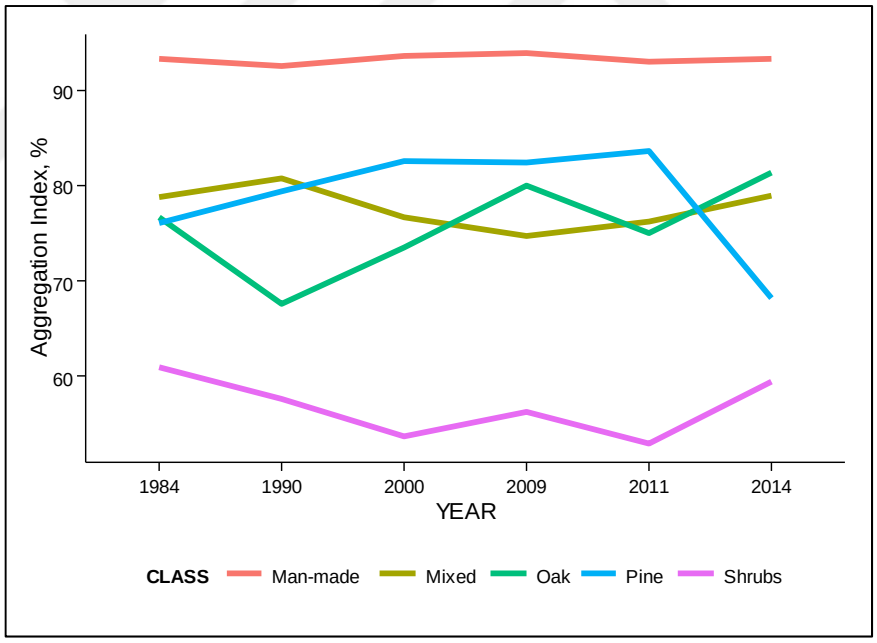

Figure 35, Evolution of AI in the multiclass classification during the period.

3.3. Regression

Twelve RF models were built by using the different databases (i.e. LO, LV, LT, and LVT) in order to predict some of the LiDAR-derived variables (CHM, CC and HMAX). Here the accuracy of each model was assessed by calculating the R^2 and the RMSE in both, OOB and the test data. Results are presented in Table 22.

Table 22. Accuracy assessment of the RF models for regression. RMSE-OOB and RMSE are expressed in the same units as the variable that represent (CHM and HMAX in m and CC in %), R^2 in %.

Variable	CHM				CC				HMAX			
Database	LO	LT	LV	LVT	LO	LT	LV	LVT	LO	LT	LV	LVT
R^2	69.42	74.03	69.39	73.46	69.30	74.60	69.31	73.98	67.54	73.90	67.30	73.40
RMSE - OOB	0.611	0.563	0.611	0.569	7.683	6.988	7.681	7.072	2.574	2.308	2.583	2.330
RMSE	0.618	0.569	0.617	0.576	7.610	6.922	7.599	6.996	2.562	2.297	2.568	2.317

The performance of all RF models can be considered as good since the proportion of variance explained in percent was ranged from 67.30% to 74.60%. In all cases the RF built with LT database achieved the highest R^2, 74.03%, 74.60% and 73.90% in CHM, CC and HMAX, respectively. Differences between RMSE and RMSE-OOB were negligible being as a maximum of 0.007m and 0.015m in CHM and HMAX, respectively and 0.083% in CC. Thus, from now on, RMSE will refer to the RMSE obtained from the test data. All models built with LT also obtained the best results regarding to RMSE. With only the spectral response variables (LO) the RMSE as slightly higher than in the other models except in HMAX in which LV database obtained the worst results. In general, the addition of topographical data to LO reduced the RMSE. In contrast the addition of vegetation

ndices (LV) did not improve the accuracy of the model but even in some cases it was slightly worsen.

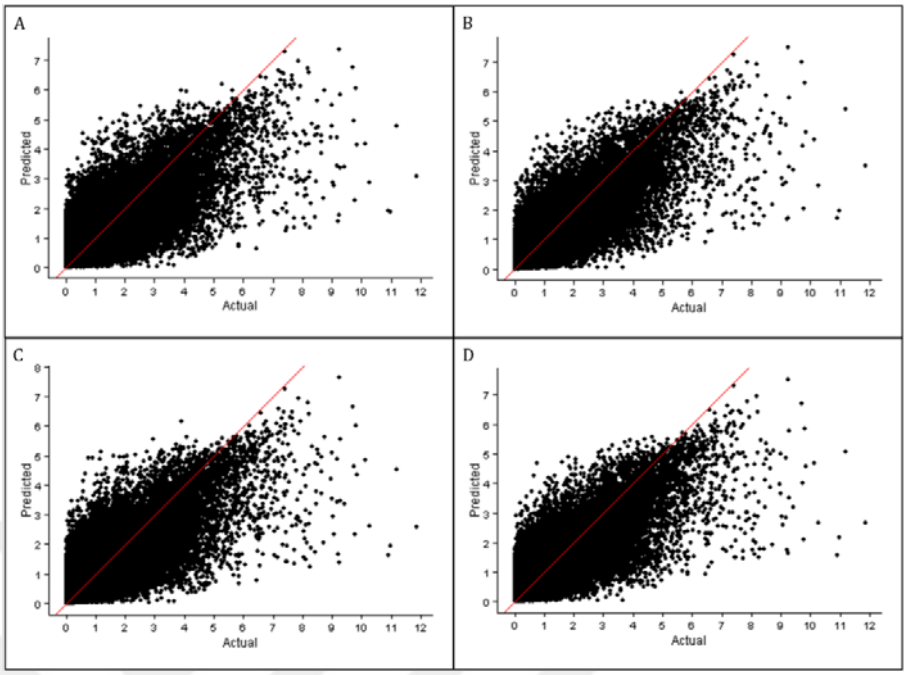

Figure **36** and Figure 38 show the actual versus predicted plots for CHM, CC and HMAX, respectively.

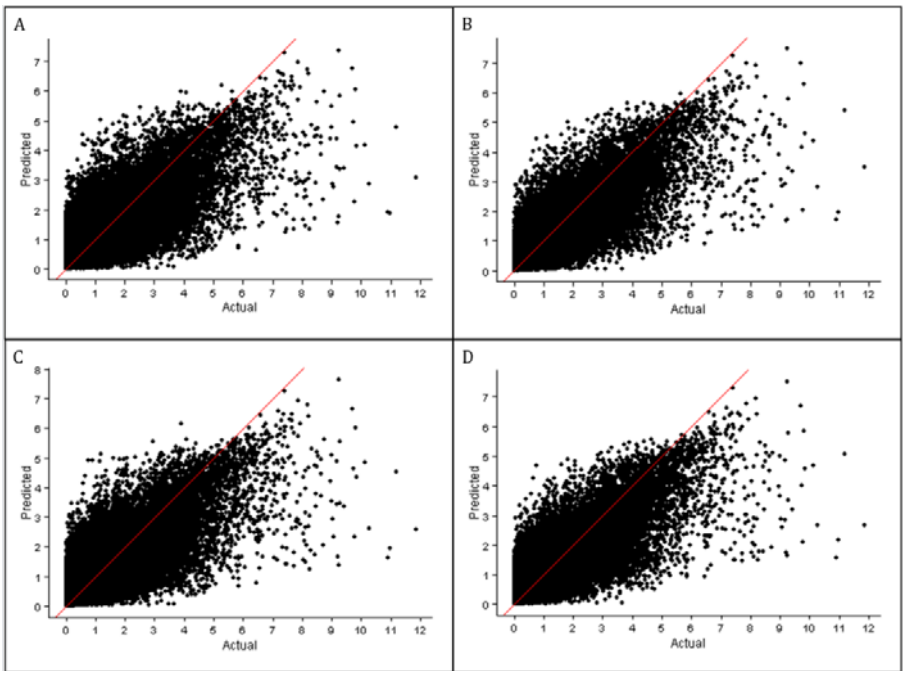

Figure 36. Actual by predicted plots of the RF models built with CHM as response variable: A) LO database, B) LT database, C) LV database, D) LVT database.

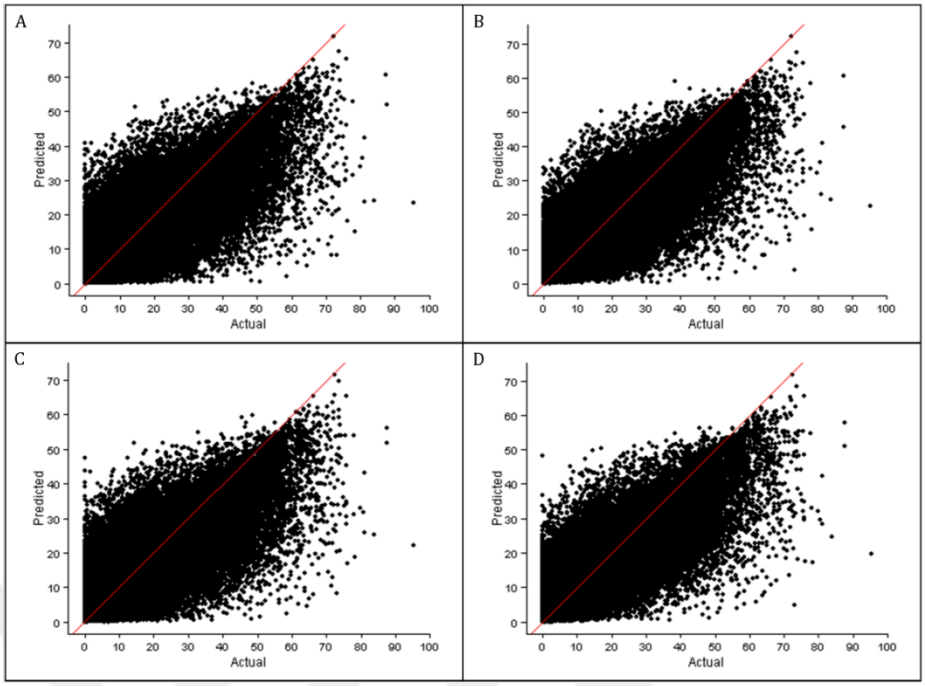

Figure 37.Actual by predicted plots of the RF models built with CC as response variable: A) LO database, B) LT database, C) LV database, D) LVT database.

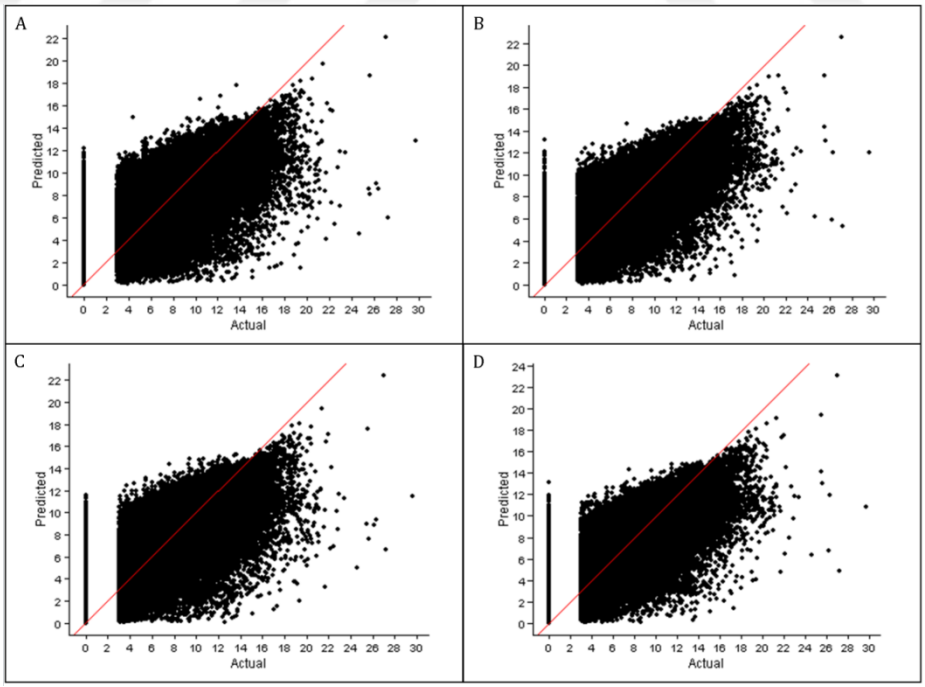

Figure 38. Actual by predicted plots of the RF models built with HMAX as response variable: A) LO database, B) LT database, C) LV database, D) LVT database.

3.3.1. Variable importance

Table 23 Table 25 show the variables shorted in descending importance in the prediction of the variables of study.

Table 23.Variable importance for the CHM prediction (shorted in descending order)

LO	LT	LV	LVT
B4	SLOPE	EVI	SLOPE
B5	ASPECT	B4	ASPECT
B2	ELEVATION	GREEN	ELEVATION
B1	B4	B5	B4
B3	B5	NDVI	EVI
B7	B3	WET	B5
	B2	SR	WET
	B1	B2	SR
	B7	B7	GREEN
		BRIGHT	NDVI
		B3	B2
		B1	B7
			B3
			B1
			BRIGHT

Table 24. Variable importance for the CC prediction (shorted in descending order)

LO	LT	LV	LVT
B4	ASPECT	EVI	ELEVATION
B5	SLOPE	GREEN	SLOPE
B1	ELEVATION	B5	ASPECT
B2	B5	NDVI	EVI
B3	B4	SR	GREEN
B7	B1	WET	B5
	B3	B1	NDVI
	B7	B7	WET
	B2	B4	SR
		BRIGHT	B7
		B2	B4
		B3	B1
			BRIGHT
			B2
			B3

Table 25. Variable importance for the CC prediction (shorted in descending order of mean decrease accuracy

LO	LT	LV	LVT
B4	ASPECT	GREEN	ASPECT
B2	ELEVATION	B4	ELEVATION
B1	SLOPE	NDVI	SLOPE
B3	B4	SR	EVI
B5	B1	EVI	NDVI
B7	B5	WET	GREEN
	B2	B5	B4
	B3	B1	SR
	B7	B2	B5
		B3	WET
		B7	B7
		BRIGHT	B2
			B1
			B3
			BRIGHT

3.3.2. Prediction of CHM

Table 26. Statistical summary of CHM (in m).shows the summary of the estimation of the CHM using Landsat imagery and topographical (LT) database.

Table 26. Statistical summary of CHM (in m).

	1984	1990	2000	2009	2011	2014
Min.	0.013	0.015	0.014	0.000	0.009	0.004
1st Qu.	0.423	0.459	0.240	0.126	0.214	0.298
Median	0.968	1.212	1.052	0.668	0.992	1.047
Mean	1.178	1.618	1.273	0.892	1.275	0.966
3rd Qu.	1.642	2.621	1.881	1.341	1.953	1.404
Max.	5.412	5.339	5.992	7.555	6.396	5.406

In Figure 39 the maps representing the prediction of CHM in the different years.

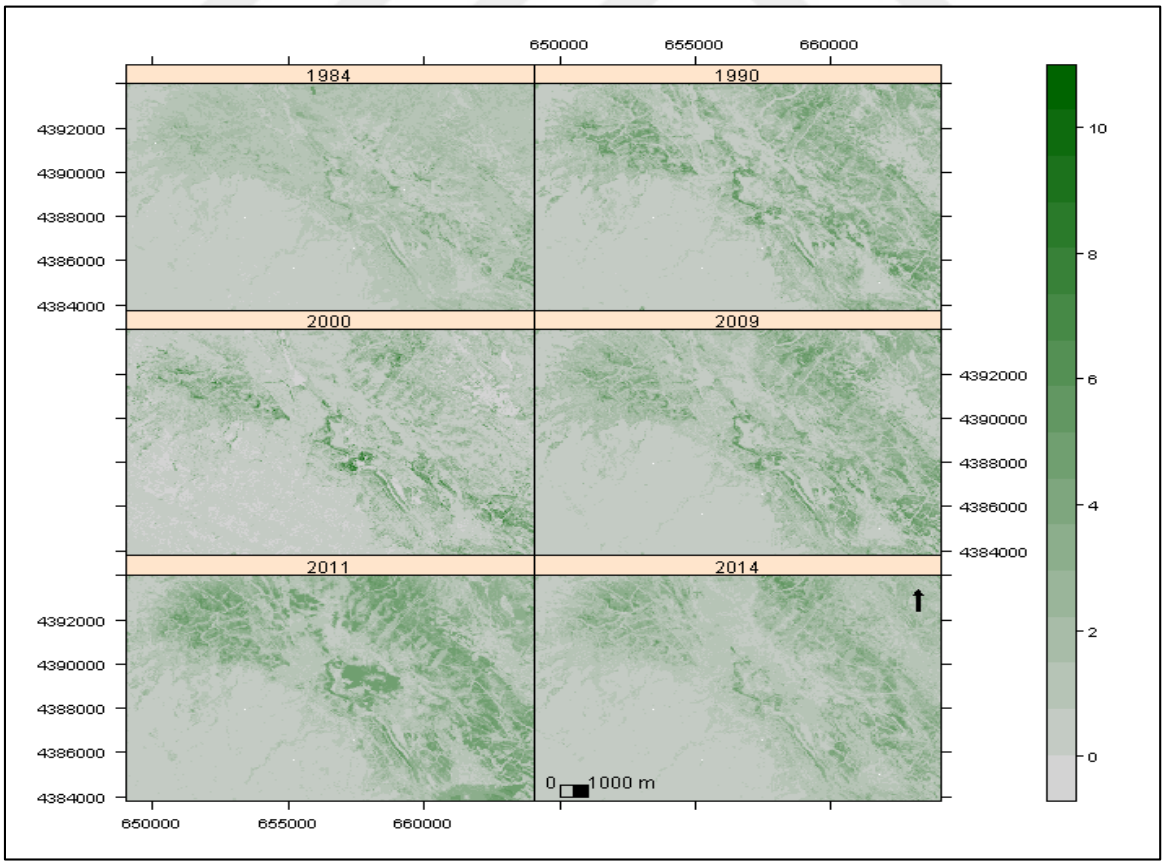

Figure 39. CHM (in m) prediction in the different years.

3.3.3. Prediction of CC

Table 26. Statistical summary of CHM (in m).shows the summary of the estimation of the CC using Landsat imagery and topographical (LT) database.

Table 27. Statistical summary of CC (in %).

	1984	1990	2000	2009	2011	2014
Min.	0.03	0.02	0.12	0	0.01	0.01
1st Qu.	5.32	6.25	4.05	1.59	2.83	2.84
Median	13.30	16.15	14.10	9.34	13.86	15.16
Mean	14.70	18.38	15.66	11.89	15.88	14.14
3rd Qu.	21.36	28.64	24.01	18.72	25.35	21.86
Max.	54.06	52.67	58.82	72.06	62.06	57.77

In Figure 40 the maps representing the prediction of CC in the different years.

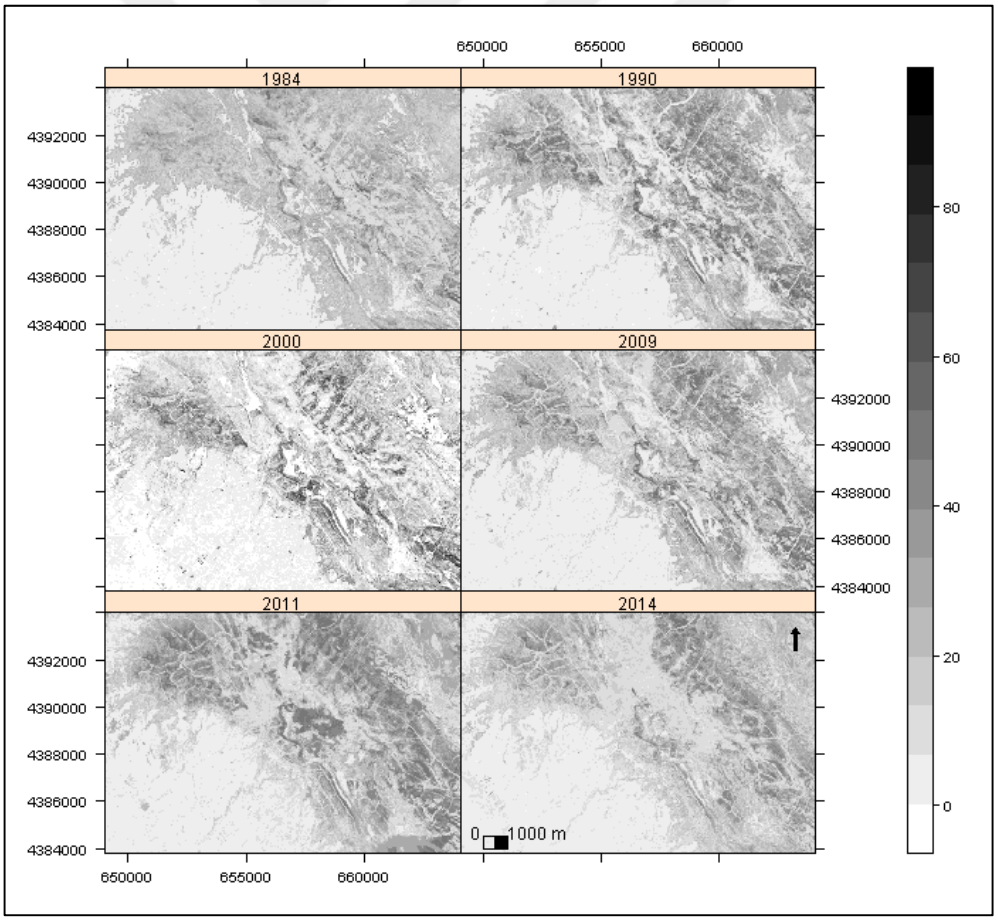

Figure 40. CC prediction in the different years

3.3.4. Prediction of HMAX

Table 26. Statistical summary of CHM (in m).shows the summary of the estimation of the HMAX using Landsat imagery and topographical (LT) database. In Figure 40 the maps representing the prediction of CC in the different years.

Table 28. Statistical summary of HMAX (in m).

	1984	1990	2000	2009	2011	2014
Min.	1.67	1.847	1.327	0	0.1108	0.4349
1st Qu.	4.492	4.91	4.027	3.436	3.7975	3.8862
Median	8.236	9.135	8.054	6.908	8.5209	7.9703
Mean	7.716	8.656	7.579	6.681	7.6427	6.9542
3rd Qu.	10.405	12.058	10.551	10.26	10.8731	9.2021
Max.	13.999	14.349	14.682	29.885	15.2207	13.9859

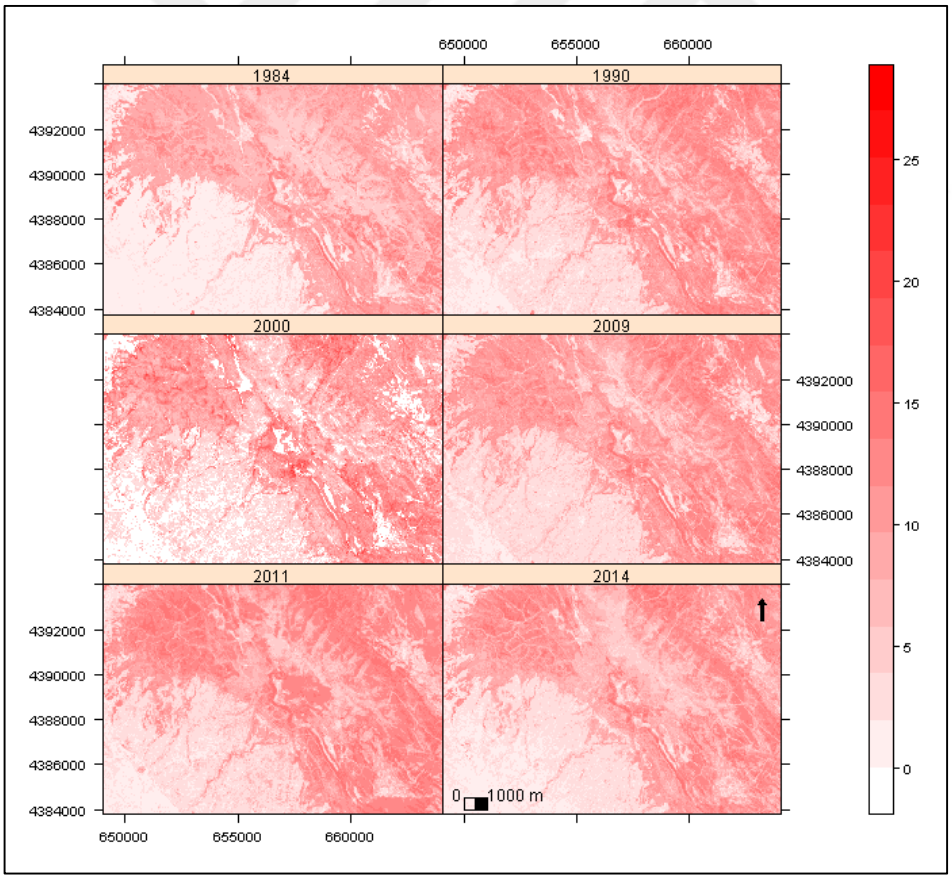

Figure 41. HMAX prediction in the different years

4. DISCUSION AND CONCLUSION

Maps used for the forest dynamics analysis were created from models whose performance was not possible to assess. A certain amount of bias was derived by the classification process. This uncertainty is derived from (i) ground reference data derived by ancillary data (ii) lack of test data, except from the 2009 (iii) preprocessing of Landsat images (iv) definition of classes, specially mixed forest that takes attributes of other two classes (vi) grain and spatial resolution (vii) very high local spectral variability due to shadows or tree cover gaps (viii) spectral resolution of the Landsat imagery and (ix) assumption that first returns in LiDAR data were capturing the top of the trees.

As pointed in (Rocchini et al. 2013) any ecosystem property has an associated error of unknown magnitude, and that the statistical quantification of uncertainty should be a core part of scientific research including using remote sensing in ecosystem mapping.

Random Forest algorithm was used for classification and regression purposes and different accuracies have been obtained. While the accuracies for classification in the forest/non-forest approach reached 98.8% and in the multiclass approach 95.35%, similar to Nourzad & Pradhan (2012) that obtained 98.9% for the binary classification and 94.6% for the multi-class classification using ensemble classification algorithms (Adaboost).

The maximum accuracies for regression purposes were 74.0% with RMSE = 0.56m, 74.6% with RMSE = 6.98% and 73.9% with RMSE = 2.3m for CHM, CC and HMAX, respectively. Classification accuracies are in concordance with other similar studies. Ahmed et al. (2015) obtained values of R^2 of 88% with RSME = 2.39m and 72% with RMSE = 0.068%, for canopy height and canopy cover, respectively, in mature forest classification using RF.

The analyzed Mediterranean landscape (Sierra de Negrete) has been managed during the last 3 decades. It showed fluctuation during the study period but landscape analysis through metrics pointed out that forest class area has been maintained during the study period. Nevertheless, it appears more fragmented since the forest NP increased about 20% during the period and the MPA underwent a drop of similar characteristics.

In the multiclass classification, the analysis suggests that Man-made class increased in area and is less fragmented with the MPA increasing about 22%. Pine class area

decreased dramatically about a 30% with an important fragmentation and reducing the LPI, MPA and the patches are less aggregated than in the beginning of the period of study.

Conversely, the management strategy of conservation of oak forest is causing the effect of increase of area and number of patches. LPI is also increasing together with MPA and AI.

The mixed forest is also being maintained in terms of area and AI but NP and LPI are lower than in 1981. On the other hand, the MPA is increasing. Shrublands changes are mainly visible in the increase of NP and the slightly decrease in LPI and MPA.

The dramatic changes that many of the metrics show in the three forest classes may be induced by the focus of the harvesting of pine trees and the conservation of oak trees. More patches of mixed forest became oak forest since the reduction of pine trees affects the spectral response of the surface in the way that the classificatory recognizes it as oak.

The addition of LiDAR-based variables to the model have increase substantially the performance of the classification but the inclusion of topographic variables resulted more important and the higher accuracy that was achieved in the FUSION of spectral, LiDAR and topographic variables. The vegetation indices did not produce a significant effect in the performance of RF for classification and for prediction purposes.

The use of topographic variables also improved the performance of RF algorithm in regression when predicting LiDAR-based features altogether with spectral-based variables.

The silvicultural activities focused on pine species for biomass production have modified the landscape by recovering Holm oak species which correspond to the potential natural vegetation of this area. The landscape in the study area became fragmented over the study period, because of the increase in the number of patches and the decrease in mean patch area.

The prediction of CHM supposed not a big indicator to assess the evolution of the canopy structure over the period. That is due in part to the resampling process that differ the original CHM data from *lastools* with a resolution of 2m and the subsequently loose of information. This is not the case of the HMAX since even suffering the resampling to 30m cell, the information of the maximum point of 225 original pixels in the 2x2 grid was not lost in the operation of averaging. Hence, this indicator could be useful to analyze the canopy. Is noticeable that the prediction of this variable is underestimated and in the year 2009 (data from *lastools*) the maximum height was about 30 m but in the prediction with RF the maximum was, in the most of the cases, lower than 15 m.

The estimation of the CC with *lascanopy* command in *lastools* in the year 2009 resulted to be as maximum 72.06 % while in the rest of the years of the study were inferior. Again, RF prediction did not performed with accuracy and not so much useful to explain forest dynamics.

The use of R statistics software provided a framework that integrates data processing, analysis and modelling. Furthermore, it was used for manipulating a huge amount of data in several formats.

The binary approach proposed in this study could be use in other areas, not only at a forest scale but also at a regional scale. It could be useful to analize the changes in the forest during the time.

5. RECOMMENDATIONS

For further studies could be interesting to gather field data in order to validate the models. In this work was received little collaboration from the government entities that manage forest of the study area. In fact, inventory data was not provided when it was required. Overcome this drawback with the limited initial resources of funds and time was difficult. As outcome, easy data access could be recommended in the future to promote the progress of the forest science.

In line with this, increase spectral resolution could allow obtaining more detailed information about the spectroradiometric properties of the landscape. As the clear cuttings are forbidden in the study area, the disturbances caused by sylvicultural treatments could be omitted.

Also LiDAR cloud-points data with a higher density would be desirable in order to reduce the uncertainty.

6. REFERENCES

Aardt, J.A.N. Van and Wynne, R.H., 2001. Spectral Separability among Six Southern Tree Species. Photogrammetric Engineering & Remote Sensing, 67 No. 12(December), pp.1367 –1375.

Ahmed, O.S., Franklin, S.E., Wulder, M.A., and White, J.C., 2015. Characterizing Stand-Level Forest Canopy Cover and Height Using Landsat Time Series, Samples of Airborne LiDAR , and the Random Forest Algorithm. ISPRS Journal of Photogrammetry and Remote Sensing, 101, 89–101.

Başkent, E.Z. and Kadioğullari, A.I., 2007. Spatial and temporal dynamics of land use pattern in Turkey: A case study in İnegöl. Landscape and Urban Planning, 81,4, 316–327.

Breiman, L.E.O., 2001. Random Forests. Machine Learning, 45, 1, 5–32.

Carreiras, J.M.B., Pereira, J.M. and Pereira, J.S., 2006. Estimation of tree canopy cover in evergreen oak woodlands using remote sensing. Forest Ecology and Management, 223, 45–53.

Chan, J.C.-W. et al., 2008. Binary Classification Strategies for Mapping Urban Land Cover with Ensemble Classifiers. IGARSS 2008 - 2008 IEEE International Geoscience and Remote Sensing Symposium, 3, 1004–1007.

Cohen, J., 1960. A coefficient of agreement of nominal scales. Educational and Psychological Measurement, 20,1, 37–46. Available at:

Coleman, T., Gudapati, L. & Derrington, J., 1990. Monitoring forest plantations using Landsat Thematic Mapper data. Remote Sensing of Environment, 33(3), pp.211–221.

Duncanson, L.I. et al., 2015. The importance of spatial detail: Assessing the utility of individual crown information and scaling approaches for lidar-based biomass density estimation. Remote Sensing of Environment, 168, pp.102–112. ESRI, 2013. ArcGIS Desktop: Release 10.2. *Redlands CA*.

Estornell, J., Ruiz, L.A. and Velázquez-Marti, B., 2011. Study of shrub cover and height using LIDAR data in a Mediterranean area. Forest Science, 57,3, 171–179.

Gamer, M., Lemon, J. and Fellos, I., 2012. irr: coefficients of interrater reliability and agreement. R package version 0.84, 1–32.

Garcia-Gutierrez, J., Gonçalves-Seco, L. and Riquelme-Santos, J.C., 2011. Automatic environmental quality assessment for mixed-land zones using lidar and intelligent techniques. Expert Systems with Applications, 38,6, 6805–6813.

Gómez, C., White, J.C., Wulder, M.A. and Alejandro, P., 2014. Historical forest biomass dynamics modelled with Landsat spectral trajectories. ISPRS Journal of Photogrammetry and Remote Sensing, 93, 14–28.

Gong, P., Wang, J., Yu, L., Zhao, Y.C., Zhao, Y.Y., Liang, L., Niu, Z.G., Huang, X.M., Fu, H.H., Liu, S., Li, C.C., Li, X.Y., Fu, W., Liu, C.X., Xu, Y., Wang, X.Y., Cheng, Q., Hu, L.Y., Yao, W.B., Zhang, H., Zhu, P., Zhao, Z.Y., Zhang, H.Y., Zheng, Y.M., Ji, L.Y., Zhang, Y.W., Chen, H., Yan, A., Guo, J.H., Yu, L., Wang, L., Liu, X.J., Shi, T.T., Zhu, M.H., Chen, Y.L., Yang, G.W., Tang, P., Xu, B., Giri, C., Clinton, N., Zhu, Z.L. Chen, J. and Chen, J.,2013. Finer resolution observation and monitoring of global land cover: first mapping results with Landsat TM and ETM+ data. International Journal of Remote Sensing, 34,7, 2607–2654.

Goslee, S.C., 2011. Analyzing Remote Sensing Data in R : The landsat Package. Journal of Statistical Software, 43,4, 1–25.

Heller, Robert C.,2014. technical coordinator 1975. Evaluation of ERTS-1 data for forest and rangeland surveys. Res. Pap. PSW-RP-112. Berkeley, CA: U.S. Department of Agriculture, Forest Service, Pacific Southwest Forest and Range Experiment Station. 67,

Robert J. Hijmans 2015. raster: Geographic Data Analysis and Modeling. R package version 2.3-33.

Horning, N., 2010. Random Forests: An algorithm for image classification and generation of continuous fields data sets. International Conference on Geoinformatics for Spatial Infrastructure Development in Earth and Allied Sciences *2010*, 1–6.

Huete, A. et al., 2002. Overview of the radiometric and biophysical performance of the MODIS vegetation indices. Remote Sensing of Environment, 83,1-2, 195–213.

Hug, C., Krzystek, P. and Fuchs, W., 2012. Advanced Lidar data processing with Lastools. In International Society for Photogrammtry and Remote Sensing (ISPRS).

Kankare, V., Vastaranta, M., Holopainen, M., Räty, M., Yu, X., Hyyppä, J., Hyyppä, H., Alho, P. and Viitala, R., 2013. Retrieval of Forest Aboveground Biomass and Stem Volume. Remote Sensing, 5, 2257–2274.

Karathanassi, V., Andronis, V. and Rokos, D., 2000. Evaluation of the Topograhic Normalization Methods for a Mediterranean Forest Area. International Archives of the Photogrammetry, Remote Sensing, XXXIII(B7), 654–661.

Leiterer, R., Furrer, R., Schaepman, M.E. and Morsdorf, F., 2015. Forest canopy-structure characterization: A data-driven approach. Forest Ecology and Management, 358, 48–61.

Liaw, A. ve Wiener, M., 2015. Package ' randomForest". Breiman and Cutler"s random forests for classification and regression. *CRAN Reference manual*.

Lu, D., Ge, H., Shizhen, H., Xu, A., Zhou, G. and Du, H, 2008. Pixel-based Minnaert Correction Method for Reducing Topographic Effects on a Landsat 7 ETM+ Image. Photogrammetric Engineering & Remote Sensing, 74,11, 1343–1350.

Martinez del Castillo, E., García-Martin, A. Longares L.A., and De Luis, M., 2015. Evaluation of forest cover change using remote sensing techniques and landscape metrics in Moncayo Natural Park (Spain). Applied Geography, 62, 247–255.

Mcgarigal, K. and Marks, B.J., 1994. Spatial Pattern Analysis Program for Quantifying Landscape Structure. In U.S. Department of Agriculture, Forest Service, Pacific Northwest Research Station , Portland, OR, 351, 1–134.

McNemar, Q., 1947. Note on the sampling error of the difference between correlated proportions or percentages. Psychometrika, 12,2, pp.153–157.

Meddens, A.J.H., Hicke, J.A., Vierling, L.A. and Hudak, A.T.., 2013. Evaluating methods to detect bark beetle-caused tree mortality using single-date and multi-date Landsat imagery. Remote Sensing of Environment, 132, 49–58.

Næsset, E., 2002. Predicting forest stand characteristics with airborne scanning laser using a practical two-stage procedure and field data. Remote Sensing of Environment, 80,1, 88–99.

Neteler, M. ve Mitasova, H., 2008. Open source GIS: A GRASS GIS approach. *Open Source GIS: A GRASS GIS Approach*, 1–406.

Nourzad, S. and Pradhan, a, 2012. Binary and Multi-class Classification of fused LIDAR-Imagery Data using an Ensemble Method. Construction Research Congress *2012*, 909–918.

Pal, M., 2005. Random forest classifier for remote sensing classification. International Journal of Remote Sensing, 26,1, 217–222.

Pebesma, E., Rowlingson, B. and Bivand, M.R.B., 2012. Package " rgdal ." *R-CRAN*, 4, 1–41.

Bivand, R., Keitt, T. and Rowlingson, B., 2015. rgdal: Bindings for the Geospatial Data. Abstraction Library. R package version 0.9-2.

R Development Core Team, R., 2011. R: A Language and Environment for Statistical Computing R. D. C. Team, ed. R Foundation for Statistical Computing, 1(2.11.1), p.409.

Rocchini, D., Foody, G.M., Nagendra, H., Ricotta, C., Anand, M., He., K.S., Amici, V., Kleinschmiti, B., Försteri, M., Schmidtleinj, S., Feilhauerl, H., Ghislaa, A., Metz, M. ve Neteler, M., 2013. Uncertainty in ecosystem mapping by remote sensing. Computers and Geosciences, 50, 128–135.

Rokach, L., 2016. Decision forest : Twenty years of research. Information fusion, 27, 111–125.

Rouse, J.W., Haas, R.W., Schell, J.A. and Harlan, J.C.,1973. Monitoring the vernal advancement and retrogradation (green wave effect) of natural vegetation, Greenbelt, MD: NASA/GSFC Type III, Final Report

Singh, K.K., Vogler, J.B., Shoemaker, D.A. and Meentemeyer, R.K. 2012, LiDAR-Landsat data fusion for large-area assessment of urban land cover: Balancing spatial resolution, data volume and mapping accuracy. ISPRS J. Photogramm. Remote Sens. 74, 110–121.

Smith, J.A., Tzeu, L.L. and Ranson, K.J., 1980. The Lambertian assumption and Landsat data. Photogrammetric Engineering & Remote Sensing, 46,10, 1183–1189.

Terradas, J., 2005. Forest dynamics: a broad view of the evolution of the topic, including some recent regional contributions. Forest Systems, 14,3,.525–537.

Thomlinson, J.R.., Bolstad, P.V.. and Cohen, B., W., 1999. Coordinating methodologies for scaling landcover classifications from site-specific to global: steps toward validating global map products. Remote Sensing of Environment, 70, 16–28.

URL-1 http://earthexplorer.usgs.gov/ 1 mart 2015

URL-2 http://centrodedescargas.cnig.es/CentroDescargas/buscadorCatalogo.do 18 mart 2015

Vanderwal J., Falconi L., Januchowski S., Shoo,L.ve Storlie,C., 2014. Package "SDMTools". Species Distribution Modelling Tools: Tools for processing data associated with species distribution modelling exercises. R-package version 1.1.221.

Vega-García, C. ve Chuvieco, E., 2006. Applying Local Measures of Spatial Heterogeneity to Landsat-TM Images for Predicting Wildfire Occurrence in Mediterranean Landscapes. Landscape Ecology, 21(4), pp.595–605.

Wickham, H., 2009. ggplot2, elegant graphics for data analysis. Springer, New York

AUTOBIOGRAPHY

I was born in Valencia the 3th November of 1981. In 2009 I started my studies of Technical Forest Engineer in the Polytechnic University of Valencia (Spain). In 2011 I spent one academic year in Mendel University of Brno (Czech Republic) were I wrote and presented publicly my final project tittled "Estimation of Aboveground Biomass of Norway Spruce [*Picea abies* (L.) Karst]" trees in managed and unmanaged mixed stands". I was awarded with the prize to the best academic records in Technical Forest Engineer by the Polytechnic University of Valencia in 2012. In 2013 I was awarded with an Erasmus Mundus scholarship to study MSc Mediterranean Forestry and Natural Resources Management. The academic course 2013/14 I studied in the University of Lleida (Catalonia, Spain). I spent the third semester of the academic year 2014/15 in the Instituto Superior de Agronomia (Lisbon, Portugal). Later, I moved to Trabzon to write this thesis in the Karadeniz Technical .